American Mineralogist, Volume 109, pages 225–242, 2024

Crystal chemistry and thermodynamic properties of zircon structure-type materials

Andrew C. Strzelecki[1,2,3,4], Xiaodong Zhao[1,2], Paul Estevenon[5], Hongwu Xu[4,6], Nicolas Dacheux[7], Rodney C. Ewing[8,†], and Xiaofeng Guo[1,2,3,9,*]

[1]Department of Chemistry, Washington State University, Pullman, Washington 99164, U.S.A.
[2]Alexandra Navrotsky Institute for Experimental Thermodynamics, Washington State University, Pullman, Washington 99164, U.S.A.
[3]Materials Science and Engineering, Washington State University, Pullman, Washington 99164, U.S.A.
[4]Earth and Environmental Sciences Division, Los Alamos National Laboratory, Los Alamos, New Mexico 87545, U.S.A.
[5]CEA, DES, ISEC, DMRC, University of Montpellier, Marcoule, 30207, France
[6]School of Molecular Sciences and Center for Materials of the Universe, Arizona State University, Tempe, Arizona 85287, U.S.A.
[7]ICSM, University of Montpellier, CNRS, CEA, ENSCM, Site de Marcoule, Bagnols sur Ceze, 30207, France
[8]Department of Earth and Planetary Sciences, Stanford University, Stanford, California 94305, U.S.A.
[9]School of the Environment, Washington State University, Pullman, Washington 99164, U.S.A.

Abstract

Zircon-class ternary oxide compounds have an ideal chemical formula of ATO_4, where A is commonly a lanthanide and an actinide, with T = As, P, Si, or V. Their structure ($I4_1/amd$) accommodates a diverse chemistry on both A- and T-sites, giving rise to more than 17 mineral end-members of five different mineral groups, and in excess of 45 synthetic end-members. Because of their diverse chemical and physical properties, the zircon structure-type materials are of interest to a wide variety of fields and may be used as ceramic nuclear waste forms and as aeronautical environmental barrier coatings, to name a couple. To support advancement of their applications, many studies have been dedicated to the understanding of their structural and thermodynamic properties. The emphasis in this review will be on recent advances in the structural and thermodynamic studies of zircon structure-type ceramics, including pure end-members [e.g., zircon ($ZrSiO_4$), xenotime (YPO_4)] and solid solutions [e.g., $Er_xTh_{1-x}(PO_4)_x(SiO_4)_{1-x}$]. Specifically, we provide an overview on the crystal structure, its variations and transformations in response to non-ambient stimuli (temperature, pressure, and radiation), and its correlation to thermophysical and thermochemical properties.

Keywords: Zircon, thermodynamics, crystal chemistry, high pressure, high temperature, lanthanides, actinides

Introduction

Ternary oxides with an ideal chemical formula of ATO_4 and tetragonal symmetry ($I4_1/amd$) are comprised of zircon structure type compounds, as they share their crystal structure with the eponymous zirconium orthosilicate mineral, zircon ($ZrSiO_4$) (Finch and Hanchar 2003). As a result of the structural flexibility of the zircon structure, the A-site can be occupied by large cations (i.e., Ca^{2+}, Er^{3+}, U^{4+}, Ta^{5+}) charge balanced by cations (i.e., Cr^{6+}, P^{5+}, Si^{4+}, B^{3+}) in the T-site. Ultimately, the structural flexibility and diverse chemistry gives rise to more than 17 mineral end-members of five different mineral groups (Berzelius 1829; Curtis et al. 1954; Stieff et al. 1955, 1956; Mrose and Rose 1961; Miles et al. 1971; Neves et al. 1974; Goldwin et al. 1976; Deliens and Piret 1986; Bernhard et al. 1998; Buck et al. 1999; Demartin et al. 2001; Finch and Hanchar 2003; Kolitsch and Holtstam 2004; Witzke et al. 2008; Schlüter et al. 2009; Moriyama et al. 2011; Baudracco-Gritti et al. 1987) and in excess of 45 synthetic synthetic ceramic end-members (Chakoumakos et al. 1994; Ni et al. 1995; Finch and Hanchar 2003; Kolitsch and Holtstam 2004). As many of these compounds exhibit complete solid solutions in both A- and/or T-site (Graeser et al. 1973; Finch and Hanchar 2003; Kolitsch and Holtstam 2004), the number of synthetic compounds through various chemical combinations on the two sites creates limitless possibilities for unusual zircon-type ceramics.

In natural systems, zircon-type minerals are common as accessory phases, which occur in various sedimentary, igneous, and metamorphic rocks. As a whole, zircon-type minerals are extremely durable with affinity to incorporate actinides and lanthanides (Weber et al. 1995). The durability of zircon-type materials is demonstrated by their high insolubility under various geochemical conditions (McMurdie and Hall 1947; Subbarao et al. 1990; Grover and Tyagi 2005) (i.e., high *P-T* environments and highly saline brines), even retaining these properties of insolubility as it undergoes radiation-induced amorphization (i.e., metamictization) (Ewing et al. 1995a; Weber et al. 1995, 2019), and high physical toughness as the mineral grains are shown to endure the abrasive nature of weathering and erosional processes. This has led to the use of several zircon-type minerals in geochronological studies, including $ZrSiO_4$ and YPO_4. The geochronological studies make use of a few different isotopic systems, including U-Th-Pb and Lu-Hf, with these two being used to derive the age of Earth (4.543Ga) (White 2015). Outside of geochronological studies,

* E-mail: x.guo@wsu.edu. Orcid 0000-0003-3129-493X
† Orcid 0000-0001-9472-4031

0003-004X/24/0002–225$05.00/DOI: https://doi.org/10.2138/am-2022-8632

the incorporation of lanthanides into the A-site of the zircon structure has proven useful in both geothermometry (Rubatto and Hermann 2007) and oxybarometry studies (Burnham and Berry 2012), while Ti incorporation in the T-site has found utility in zircon thermometry (Watson et al. 2006).

Because of the high loading of *f*-elements (lanthanides and actinides), durability, and demonstrated long-term stability, zircon-type materials have been proposed as potential ceramic-based waste forms for the immobilization of actinides associated with the nuclear fuel cycles (Boatner et al. 1980, 1984; Ewing et al. 1995a, 1995b; Ewing 1999), which include actinides from spent nuclear fuel discharged from reactors and plutonium from dismantled nuclear weapons (Burns et al. 2012). Currently, many countries are investigating ceramic waste forms to immobilize actinides prior to final disposal (Orlova and Ojovan 2019). If a zircon-type waste form is used, the immobilization step would be accomplished by incorporating actinides into its crystal structure and then storing the ceramic waste form in either a deep-mined geologic repository or deep bore-hole (Weber et al. 2009, 2019; Goel et al. 2019; Wegel et al. 2019). As zircon has been shown to be a durable mineral able to immobilize Th and U over geologic timescales that stretch well beyond hundreds of million years (White 2015), it addresses the concerns for the long-term safety associated with the integrity of a disposal system on timescales that range from thousands to tens of hundreds of thousands of years (Ewing 2015). These same thermophysical properties, which support the durability of zircon under geologic conditions, find applicability in applied material science. For instance, zircon-type silicates have been proposed as environmental and thermal barrier coatings (Hikichi and Nomura 1987; Gavrichev et al. 2006, 2010b, 2012a, 2013a; Tyurin et al. 2020).

In summary, zircon and zircon-type materials are of interest to a wide variety of fields. To support advancement of their applications, many studies have been dedicated to the understanding of their structural and thermodynamic properties. Several previous reviews have already presented basic structural knowledge and chemistry of zircon materials in the fields of geology, geochemistry, and mineralogy (Speer 1980a; Speer and Cooper 1982; Bowring and Schmitz 2003; Cherniak and Watson 2003; Corfu et al. 2003; Davis et al. 2003; Ewing et al. 2003; Finch and Hanchar 2003; Hanchar and Watson 2003; Hoskin and Schaltegger 2003; Ireland and Williams 2003; Nasdala et al. 2003; Valley 2003; Kolitsch and Holtstam 2004; Harley and Kelly 2007; Kohn et al. 2017), along with complementary reports of their thermophysical and thermodynamic properties (e.g., coefficient of thermal expansion) (Bayer 1972; Subbarao et al. 1990). The focus of this review will be devoted to recent advances in the structural and thermodynamic understanding of zircon-type materials, which include pure end-members [e.g., stetindite ($CeSiO_4$), coffinite ($USiO_4$)] and solid solutions (e.g., $U_xTh_{1-x}SiO_4$). Specifically, we provide an overview on the crystal structure, its derivation due to chemical substitution and hydrostatic pressure, and correlation to the material's thermophysical and thermochemical properties. This review aims to help researchers with this up-to-date knowledge on zircon-type materials and to continue promoting their applications, such as ceramic nuclear waste hosts and aeronautical environmental barrier coating.

Studies of synthetic zircon structure compounds

Preparation of pure zircon phase materials is critical for the study of their structures and thermodynamics. Many early landmark studies on zircon and other zircon-types materials were conducted on natural samples (Hazen and Finger 1979; Robie and Hemingway 1995), as well as synthetic single crystals (Hazen and Finger 1979; Begun et al. 1981; Milligan et al. 1982, 1983; Ellison and Navrotsky 1992; Loong et al. 1993; Robie and Hemingway 1995; Mullica et al. 1996a, 1996b; Jellison et al. 2000; Guedes et al. 2001; Ushakov et al. 2001a; Boatner 2002; Hirano et al. 2002a; Hirano et al. 2002b; Finch and Hanchar 2003; Moura et al. 2004; Mazeina et al. 2005; Dorogova et al. 2007; Santos et al. 2007). Although single crystals are the ideal samples for the determination of crystal structure via single-crystal diffraction techniques (Taylor and Ewing 1978; Chakoumakos et al. 1994; Ni et al. 1995), the variety of compounds available for these characterizations is limited by the chemical routes that allow their synthesis.

Preparing polycrystalline samples by "soft" hydrothermal synthesis (Estevenon et al. 2018, 2020a, 2020b, 2021a), can create conditions that facilitate the crystallization of metastable phases, such as $USiO_4$ (Pointeau et al. 2009; Costin et al. 2011; Labs et al. 2014; Mesbah et al. 2015), $CeSiO_4$ (Estevenon et al. 2019b, 2019a), and $PuSiO_4$ (Estevenon et al. 2020b, 2021b). Obtaining polycrystalline samples also facilitates thermodynamic measurements (i.e., enthalpy of dissolution) (Guo et al. 2016a), and enables the determination of thermodynamic parameters of the above metastable phase for the first time (Guo et al. 2015; Szenknect et al. 2016; Strzelecki et al. 2020b). The key point of this approach is to ensure the overall purity of these synthetic polycrystalline samples, which is a challenge (Estevenon et al. 2020b). While many of the synthesis methods are inspired by those previously used by Hoekstra and Fuchs (Hoekstra and Fuchs 1956; Fuchs and Hoekstra 1959) or Keller (1963) in the 1950s to the 1960s, crucial advances have recently been made in zircon-type silicate synthesis under "soft" hydrothermal conditions (≤523 K), rendering them more accessible to thermochemical characterization (Estevenon et al. 2018, 2019a, 2019b). The experimental approach considered is defined by a strict framework of the parameters (e.g., precursors, concentration, co-reactants, pH, temperature, pressure, synthesis time), allowing the formation of the target compound. Contrary to high-temperature synthesis routes, which generally have led to thermodynamically stable products at the conditions considered, hydrothermal syntheses might promote the formation of metastable kinetic reaction products depending upon the initial conditions chosen. Additionally, hydrothermal treatment generally promotes the formation of relatively well-crystallized species, facilitating their characterization. Moreover, when the selected chemical conditions were insufficient to obtain a pure final phase, syntheses might be complemented by chemical post-treatments, such as acidic and alkaline washes for $USiO_4$ syntheses (respectively allowing UO_2 and SiO_2 dissolution) (Mesbah et al. 2015).

Crystal chemistry of zircon structure compounds

Crystal structure

Zircon structure types possess a tetragonal symmetry (Fig. 1). The space group according to the international notation, also

known as Hermann-Mauguin, is $I4_1/amd$, and the corresponding Schönflies notation is D_{4h}. The extended version of the international notation would be $I4_1/a\ 2/m\ 2/d$, where one can see that these crystals are body-centered, possessing a fourfold screw axis parallel to the *a*-axis, with a twofold axis of rotation perpendicular to a mirror plane, and another twofold axis of rotation perpendicular to a diamond glide plane. Within the zircon structure, both the A-site and T-site cations occupy special positions with the site symmetry $\bar{4}2m$, including (0, ¾, ⅛) for A-site and (0, ¼, ⅜) for T-site. O atoms do not occupy a special position, exhibiting a site symmetry of *m,* located at (0, Y, Z), which is the only position that must be refined in diffraction studies. Substances possessing the zircon structure are referred to as "ortho-" and corresponding T-site anion (i.e., silicate, borate, phosphate). For instance, $ZrSiO_4$ is an orthosilicate, meaning that the silicate tetrahedra are not connected to one another, and YPO_4 is an orthophosphate. Because the TO_4 tetrahedra are not connected, the corners are joined at edges with an MO_8 dodecahedra. The arrangement of TO_4 tetrahedra and MO_8 dodecahedra can be depicted as two intersecting disphenoidal MO_4: edge-sharing $MO1_4$ alternating with TO_4 along the *c*-axis that has a longer coordinated oxygen bond and thus referred to as the extended tetrahedra, and shorter coordinated oxygen bonded compressed tetrahedra $MO2_4$ corner-sharing with another $MO2_4$ tetrahedra forming a zigzag chain along the *a*-axis (Fig. 1) (Speer 1980a; Finch and Hanchar 2003; Marcial et al. 2021).

Owing to the arrangement of the metal polyhedra, the zircon structure is comparatively open, in contrast to structural types, such as scheelite ($I4_1/a$) or monazite ($P2_1/n$) (Clavier et al. 2011). The zircon-type structure has both channels running parallel to the [001] (Fig. 1b) and small voids existing between the TO_4 and MO_8 polyhedra, which can also be viewed as potential interstitial sites for the incorporation of impurity elements. While impurities, such as He, can reside in the interstitial sites, it is much more common for impurities to be introduced through substitution of cations in either the TO_4 (e.g., Ga^{3+}, Ti^{4+}, W^{6+}) or MO_8 (e.g., Na^+, Sr^{2+}, Zn^{2+}) sites (Speer 1980b). Additionally, water molecules can also be incorporated to considerable levels, sometimes >0.5 mol per formula unit (Guo et al. 2015; Shelyug et al. 2021; Strzelecki et al. 2021, 2022). The water molecules are confined to the [001] structural channels, as initially hypothesized by Janeczek (1991) and Kijkowska (2003) and experimentally verified by Strzelecki et al. (2021, 2022) on zircon-structured orthosilicates and orthophosphates. Shelyug et al. (2021) also confirmed the confined water in orthosilicates-orthophosphates solid solutions $Th_xEr_{1-x}(SiO_4)_x(PO_4)_{1-x}$, again suggesting the commonality of the channel water in zircon-type materials. Water molecules confined in the [001] channel have significant effects on both the dehydration and structural response on heating (Shelyug et al. 2021; Strzelecki et al. 2021, 2022).

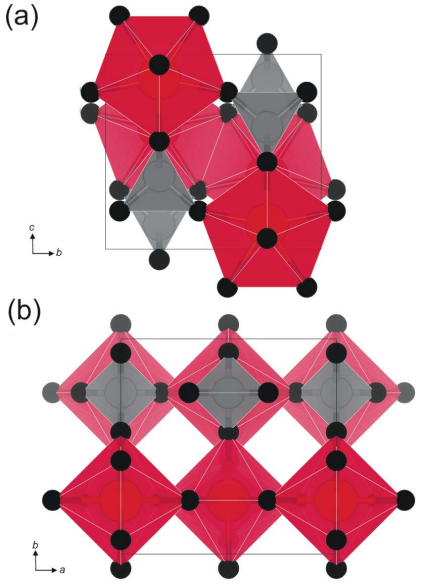

Figure 1. Projections of the tetragonal zircon structure down to **a** and **c** axes [prepared using the VESTA 3 software package (Momma and Izumi 2011)]. In both **a** and **b**, the crimson dodecahedra are MO_8, the gray tetrahedra are TO_4, and the black spheres are oxygen. (**a**) Representation of the structure along [100]. (**b**) Illustration of the structure along [001]. The figure is based on the structure reported by Robinson et al. (1971) and Speer (1980b). (Color online.)

Element substitutions in zircon structure compounds

The atomic-scale structure, although topologically rigid, is quite flexible in terms of the allowed chemistries. This is demonstrated by the large number of natural minerals and synthetic compounds that exhibit the zircon structure through variance in either the A-site or T-site. There are 17 natural minerals possessing the zircon structure. These include the orthosilicate minerals: zircon, hafnon ($HfSiO_4$), stetindite ($CeSiO_4$), thorite ($ThSiO_4$), coffinite ($USiO_4$), and uranothorite ($U_xTh_{1-x}SiO_4$); the orthophosphate minerals: xenotime (YPO_4 and $YbPO_4$) and pretulite ($ScPO_4$); the orthovanadate minerals: wakefieldite ($CeVO_4$, $LaVO_4$, $NdVO_4$, and YVO_4) and dreyerite ($BiVO_4$); the orthoarsenate minerals, chernovite ($YAsO_4$); the orthoborate minerals: behierite ($TaBO_4$) and schiavinatoite ($NbBO_4$); and the orthochromate mineral, chromatite ($CaCrO_4$) (Berzelius 1829; Curtis et al. 1954; Stieff et al. 1955, 1956; Mrose and Rose 1961; Miles et al. 1971; Neves et al. 1974; Goldwin et al. 1976; Deliens and Piret 1986; Bernhard et al. 1998; Buck et al. 1999; Demartin et al. 2001; Finch and Hanchar 2003; Kolitsch and Holtstam 2004; Witzke et al. 2008; Schlüter et al. 2009; Moriyama et al. 2011; Baudracco-Gritti et al. 1987). All these minerals exist as a continuum of solid solutions in both the A- and T-sites. Several of the end-members are strictly synthetic, in particular end-members containing REE heavier than Nd (i.e., Sm-Lu), with the notable exception of xenotime-(Yb). Additionally, there are also a few common synthetic compounds that crystallize in the zircon structure but have not yet been found to exist in nature, which include Th orthogermanate ($ThGeO_4$) and the REE orthochromates ($REECrO_4$).

The 17 mineral end-members show that the MO_8 dodecahedra of the A-site can be filed by aliovalent elements, from divalent Ca^{2+} to pentavalent Ta^{5+}, with corresponding charge balance obtained at the T-site. The ratio of the radius of the A-site to the T-site (r_A/r_T) ranges from 2.08 for hafnon to 6.73 for behierite. The variation of the unit-cell parameters of all the above compounds is represented as a function of r_A/r_T in Figure 2. All lattice parameters used in Figure 2 are further tabulated in Online

Materials[1] Table S1. There is a general clustering that emerges such that most of the compounds with the zircon structure have a r_A/r_T value between 2 and 4. Two outliers are HREE orthophosphate (xenotime) and orthoborate (behierite and schiavinatoite). In addition, LREE orthophosphates, which more commonly adopt the monazite structure ($P2_1/n$), also contribute to a very narrow range in r_A/r_T because Gd, Tb, and Dy can also be crystallized as xenotime (Ushakov et al. 2001a; Clavier et al. 2011, 2018). Likewise, when considering the alkali orthochromates, $MgCrO_4$, $CaCrO_4$, $SrCrO_4$, and $BaCrO_4$, it is worth noting that the stability of the zircon-type structure is highly sensitive to the r_A/r_T value as only $CaCrO_4$ (r_A/r_T = 4.31) crystallizes with the zircon-structure (Weber and Range 1996). The other three alkali orthochromates, i.e., $MgCrO_4$ (r_A/r_T = 3.42), $SrCrO_4$ (r_A/r_T = 4.85), and $BaCrO_4$ (r_A/r_T = 5.46), crystallize with the chromium orthovanadate structure (*Cmcm*), the monazite structure, and the barite structure (*Pnma*), respectively (Muller et al. 1969; Lentz et al. 1986; Gleissner et al. 2016).

Besides the many end-member compounds, natural zircon-structure minerals exist dominantly as solid solutions. Ionic radii with approximately similar lengths for cations with the same charge generally cause minor structural adjustments. Their mixing along the join is usually close to ideal mixing, which can be described by Vegard's law. Vegard's law is an approximate empirical rule that states that the variation of lattice parameters between two compositional isostructural end-members is linear (Denton and Ashcroft 1991). An exception is when 5*f*-block cations, Th^{4+} (1.19 Å) and U^{4+} (1.14 Å), forming a complete zircon-structure solid solution, results in strong nonideal mixing behavior (Guo et al. 2016a; Marcial et al. 2021). From a structural point of view, the cationic sublattice is very similar to that of the zircon structure with randomized U and Th, but the coordinated oxygen atoms deviate from their anionic lattice, which leads to distorted $MO1_4$ and $MO2_4$. Such polyhedral distortions originate from the electron and bonding configurations of the metal cation and the oxygen. U-O bonding shows more partial covalency due to the $5f^2$ electrons of U^{4+} along the *a*-*b* plane, while Th-O bonding is completely ionic. Hence, the relative size of $MO1_4$ and $MO2_4$ in their end-member phases (coffinite vs. thorite) are different (Marcial et al. 2021). Mixing of U and Th thus leads to homogenization of the two metal tetrahedra that are distorted as compared to the end-member structures.

Crystal chemistry of zircon-type structures under non-ambient conditions

As zircon-type materials are of interest to applications in a large variety of fields where extreme conditions are frequently encountered, including the geosciences where elevated pressure

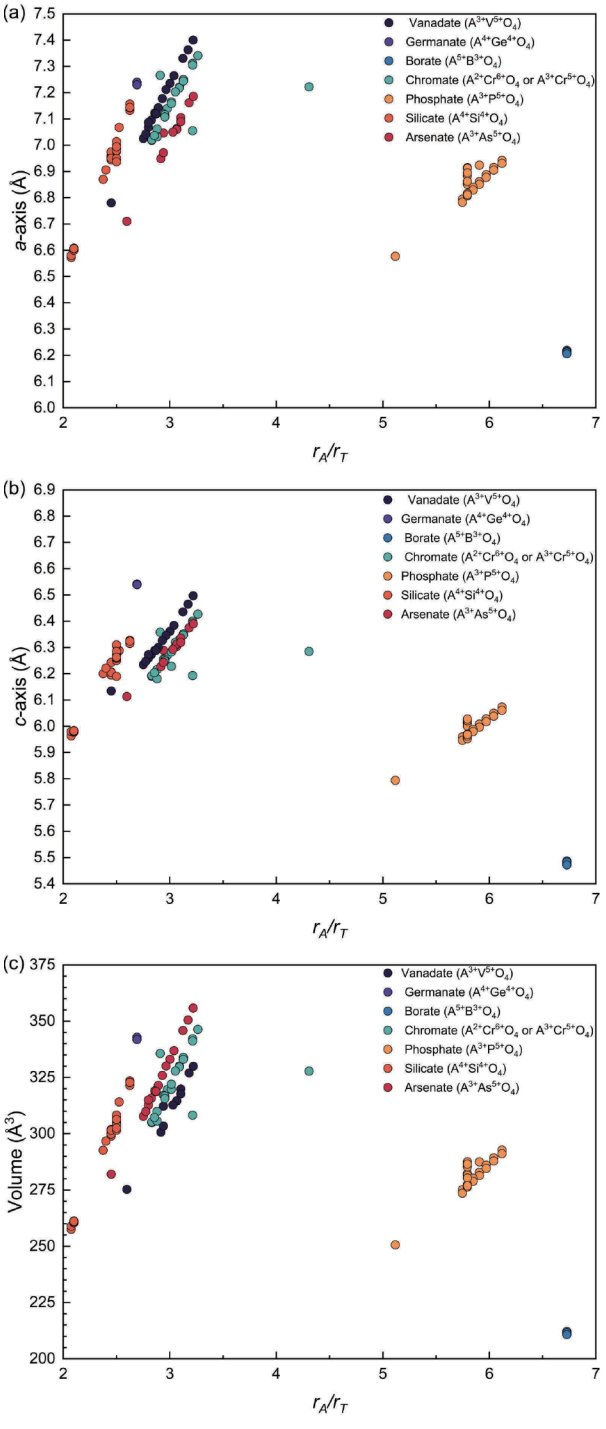

▶ **Figure 2.** Variations, as a function of the r_A/r_T, in the unit-cell parameters (**a**) *a*, (**b**) *c*, and (**c**) volume *V* for various zircon-structure materials (Hoekstra and Fuchs 1956; Stieff et al. 1956; Keller 1963; Darnley et al. 1965; Miles et al. 1971; Robinson et al. 1971; Schafer and Will 1971; Lohmüller et al. 1973; Mulak 1977; Taylor and Ewing 1978; Hazen and Finger 1979; Schäfer et al. 1979; Kusaba et al. 1985; Ennaciri et al. 1986; Fuhrmann and Pickardt 1986; Range et al. 1988, 1996; Knittle and Williams 1993; Chakoumakos et al. 1994; Ni et al. 1995; Mullica et al. 1996a; Weber and Range 1996; Jiménez et al. 2000; Skakle et al. 2000; Demartin et al. 2001; Konno et al. 2001; Tezuka and Hinatsu 2001; Ushakov et al. 2001a; Tezuka et al. 2002; Sáez-Puche et al. 2003; Ono et al. 2004a; Tange and Takahashi 2004; Van Westrenen et al. 2004; Kang and Schleid 2005; Kang et al. 2005; Schmidt et al. 2005; Achary et al. 2007; Long et al. 2007; Climent et al. 2009; Golbs et al. 2009; Pointeau et al. 2009; Sáez Puche et al. 2009; Wang et al. 2010; Reynolds 2013; Labs et al. 2014; Guo et al. 2015; Mesbah et al. 2016; Szenknect et al. 2016; Ledderboge et al. 2018; Estevenon et al. 2019a, 2019b; Bandiello et al. 2020; Strzelecki et al. 2021; Ehlers et al. 2022). (Color online.)

(*P*) and temperature (*T*) environments are prevalent, the crystal chemistry of these materials has been investigated as a function of *P* and *T*. In addition to these two intensive thermodynamic variables, the effects of radiation damage on the crystalline structure have also been investigated.

Pressure. Under either static or dynamic compression, two possible pressure-induced phase transitions can be observed for zircon structure-type materials. The first one is a reconstructive transformation to the scheelite structure, which has been observed in nearly all orthosilicates ($ZrSiO_4$, $HfSiO_4$, $CeSiO_4$, and $USiO_4$) (Reid and Ringwood 1969; Hazen and Finger 1979; Knittle and Williams 1993; Farnan et al. 2003; Gucsik et al. 2004; Ono et al. 2004a, 2004b; Tange and Takahashi 2004; Manoun et al. 2006; Luo and Ahuja 2008; Bose et al. 2009; Zhang et al. 2009; Bauer et al. 2014; Stangarone et al. 2019; Strzelecki et al. 2023), a few orthophosphates ($ScPO_4$, $YbPO_4$, and $LuPO_4$) (Zhang et al. 2008a; Lacomba-Perales et al. 2010), the majority of the orthovanadates ($REEVO_4$, REE = Sc, Y, Sm-Lu) (Wang et al. 2004; Errandonea et al. 2011, 2014; Huang et al. 2012b; Garg and Errandonea 2015; Panchal et al. 2015; Ruiz-Fuertes et al. 2018), and a single orthogermanate (β-$ThGeO_4$) (Errandonea et al. 2009a). Another possible transition is the transformation to the monazite structure, which has been demonstrated for the majority of the orthophosphates ($REEPO_4$, REE = Y, Tb-Tm) (Stavrou et al. 2008; Lacomba-Perales et al. 2010; López-Solano et al. 2010; Gomis et al. 2017) and for a few orthovanadates ($CeVO_4$, $PrVO_4$, and $NdVO_4$) (Errandonea et al. 2011; Panchal et al. 2011b; Errandonea 2015).

The zircon-to-scheelite phase transformation is a first-order (Errandonea and Garg 2018) transition and thus is reconstructive (Buerger 1961; West 2014). This is evident because the positions and site symmetries of all atoms in the unit cell are rearranged. Deformation studies on the zircon to scheelite transformation imply the slip of planes, with the dominate slip occurring along 100{001}, but the slip does not result in a change in the coordination number of either the A-site or the T-site cations (Yue et al. 2016). This is shown by the scheelite structure, where both the A-site and T-site cations occupy special positions, (0, ¼, ⅝) and (0, ¼, ⅛), respectively, with a site symmetry of $\bar{4}$. O atoms do not occupy a special position, exhibiting a site symmetry of 1, and are located at the general position (X, Y, Z). The rearrangement of the metal polyhedra from zircon to scheelite results in a ~10% increase in the overall density, with the [001] channels of zircon structure-type being completely closed in a scheelite structure-type (Finch and Hanchar 2003; Du et al. 2012). An important consequence of a reconstructive phase transition is that the high-pressure phase is quenchable. Nature also provides an example of the quenchable $ZrSiO_4$ scheelite phase, as it was found in the ejecta associated with meteorite impacts; the approved name of this high-pressure phase is reidite (Glass et al. 2002).

In addition to the zircon → scheelite phase transformation, there is a newly discovered intermediate phase, namely the high-pressure, low-symmetry (HPLS) phase ($I\bar{4}2d$) (Mihailova et al. 2019; Stangarone et al. 2019). The discovery of this intermediate phase was first predicted by a computational study (Stangarone et al. 2019) and then confirmed experimentally by Raman spectroscopy (Mihailova et al. 2019) and synchrotron X-ray diffraction (Strzelecki et al. 2023). This phase is a result of the slight rotation of the SiO_4 tetrahedra due to a softening of $B1_u$ vibrational mode to become an imaginary phonon mode at ~20 GPa (Stangarone et al. 2019). The HPLS phase has a softer bulk modulus, which may trigger a further transition to scheelite (Mihailova et al. 2019; Stangarone et al. 2019; Strzelecki et al. 2023). Moreover, our unpublished density functional theory (DFT) work on $CeSiO_4$ also discovered an imaginary phonon mode between 12 and 16 GPa, which further suggests that the phase transition to HPLS is the result of an elastic instability (Strzelecki et al. 2023). Further investigation on elastic constants is needed to determine whether the phase transition is due to shear deformation or an atomic distortion. Furthermore, additional phase transitions may also exist beyond the scheelite transformation (Errandonea et al. 2011; Garg and Errandonea 2015; Errandonea and Garg 2018), such as scheelite → fergusonite (*I*2/*a*) (Errandonea et al. 2011; Garg and Errandonea 2015; Errandonea and Garg 2018). Such a transition is a result of distortions of metal polyhedra and small translations of cations off their special position (Errandonea and Garg 2018). There is no change in the coordination number of polyhedra during the scheelite to fergusonite transition. Lastly, the $KAlF_4$ (*P*4/*mmm*) structure has been hypothesized as another potential polymorph of $ZrSiO_4$ after the scheelite phase transition but has yet to be verified experimentally (Hazen and Finger 1979; Speer and Cooper 1982).

Another route for the high-pressure transition of zircon is to monazite, which is also a first-order transition with metal polyhedra reconstructively rearranged in the unit cell such that it leads to an increase of the coordination number from eight (MO_8) to nine (MO_9). In addition, the TO_4 units in the monazite structure share edges with MO_9 units (Finch and Hanchar 2003; Clavier et al. 2011). The site symmetry in the monazite structure is greatly reduced to 1, and none of the atoms are located at special positions. The phase transition process from the zircon to monazite structure involves the rotation of the TO_4 units, a sideways movement of the (100) plane of zircon (Errandonea and Garg 2018), and a breaking of the <M-O> bond followed by the formation of two additional <M-O> bonds in the equatorial plane (Clavier et al. 2011; Errandonea and Garg 2018), leading to a decrease in compressibility. This is also reflected in a monazite structure that is denser than the zircon structure, as the [001] channels are eliminated in monazite. Furthermore, an additional phase transformation beyond monazite has been proposed as post-monazite, the identity of which is less well-defined (Panchal et al. 2015) and arguably possesses the barite structure (*Pnma*) (Lacomba-Perales et al. 2010; Errandonea et al. 2011; Errandonea 2017; Errandonea and Garg 2018; Heuser et al. 2018).

The divergence of the high-pressure phase transition of zircon may also be interpreted from a crystal-chemical perspective. In the zircon → scheelite transition, the ratio of r_A/r_T is small (e.g., having a small A-site metal cation or a large T-site cation), allowing the shifting of atoms to accommodate the increased repulsive and steric stress upon compression, compared to a large r_A/r_T ratio that triggers a zircon → monazite transition. This hypothesis has been supported by DFT calculations of orthovanadates (MVO_4, M = Y, Yb, Lu, Nd), where Panchal et al. (2015) computed the electronic structures up to 20 GPa. They demonstrate that during the zircon → scheelite transition, there is a collapse of the

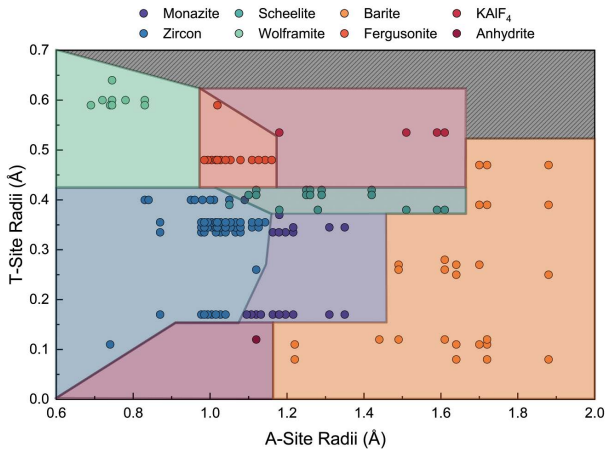

Figure 3. Bastide diagram for ATX_4 compounds. The coordination number for the A-sites for the following structure-types are sixfold for the wolframite structure-type; eightfold for the zircon, scheelite, fergusonite, $KAlF_4$, and anhydrite structure-types; ninefold for the monazite structure-type; and 12-fold for the barite structure-type. The coordination number for the T-sites for the following structure types are fourfold for monazite, zircon, scheelite, barite, fergusonite, and anhydrite; and sixfold for wolframite and $KAlF_4$. The ionic radii of the A-site and T-site cations are those reported in the literature for the appropriate coordination number for the given structure-type (Shannon 1976). (Color online.)

electronic band structure that could introduce extra stabilization energy with more electrons populating the lower energy states (Panchal et al. 2011a). In the zircon → monazite transition, the eight-coordinated polyhedra, MO_8, become unstable and require the breaking of a <M-O> bond followed by the formation of two additional <M-O> bonds in the equatorial plane (Clavier et al. 2011; Errandonea and Garg 2018).

This can further be explained through Bastide's rules of chemical pressure (Bastide 1987). These rules state that the intensive thermodynamic variable of pressure is equivalent to that of the chemical pressure, the latter of which is usually induced by, but limited to, chemical substitution, nanoparticle surface modification, and epitaxial crystal growth (Hazen 1977; Bastide 1987; Prieur et al. 2020; Lü et al. 2021; Dong et al. 2022). Previously, Bastide diagrams have been used as an effective approach for explaining observed pressure-induced phase transitions (Manjón et al. 2006a, 2006b; Errandonea and Manjón 2008; López-Solano et al. 2010; Errandonea 2017; Errandonea and Garg 2018; Heuser et al. 2018). In Bastide diagrams (Fig. 3), one plots the ionic radii of the A-site on the *x*-axis and the ionic radii of the T-site on the *y*-axis, which creates stability landscapes for different structures. In Figure 3, we have included other ternary compounds (ATX_4) that are related to the zircon structure. These related structures include those of scheelite, fergusonite, monazite, barite, wolframite (*P*2/*c*), anhydrite (*Amma*), and $KAlF_4$. The pressure-induced phase transitions that a ternary oxide is likely to go through upon compression tend to be at the top-right side of the diagram. Examples of this are shown in rare earth orthovanadate and rare earth orthophosphate systems under ambient conditions. There is a phase boundary that is defined as a function of the ionic radii of the A-site metal cation for the monazite structure compounds, including $LaVO_4$ and $LREEPO_4$ (LREE = La-Gd), as compared with those of the zircon structure compounds, $REEVO_4$ (REE = Ce-Lu) and $HREEPO_4$ (HREE = Sc, Y, and Tb-Lu). For the rare earth orthovanadates, the ionic radii define a hard cut-off between $LaVO_4$ and $CeVO_4$. This is slightly different from that of the rare earth orthophosphates, as $GdPO_4$, $TbPO_4$, and $DyPO_4$, which all exist as polymorphs of either monazite or xenotime (Ni et al. 1995; Ushakov et al. 2001a; Clavier et al. 2018; Musselman et al. 2018), but this should be viewed as a high-temperature phase transition from monazite to xenotime, which is discussed in the following section.

Temperature. Temperature-induced phase transformations of ternary oxides can be approximately viewed as the reverse process of the pressure-induced phase transition (Hazen 1977) because of thermal expansion. At high temperatures, there are irreversible phase transitions from scheelite to zircon and from monazite to zircon. Using the Bastide diagram (Fig. 3), the path for the phase transition is toward the bottom-left across the diagram. The scheelite to zircon phase transition has been observed in $ThGeO_4$, as it exhibits two polymorphic forms at ambient pressure, α-$ThGeO_4$ (scheelite structure) and β-$ThGeO_4$ (zircon structure). The α → β transition occurs above 1473 K (Achary et al. 2007; Errandonea et al. 2009a). The monazite to zircon phase transition has been reported for three rare earth orthophosphates, $GdPO_4$, $TbPO_4$, and $DyPO_4$ (Ni et al. 1995; Ushakov et al. 2001a; Clavier et al. 2018; Musselman et al. 2018). These three orthophosphates can exist as either the monazite or xenotime structures, the latter of which is more stable for Gd, Tb, and Dy at high temperatures (Ushakov et al. 2001a; Clavier et al. 2018; Musselman et al. 2018). Once the zircon structure is formed, most materials do not exhibit further phase transitions at higher temperatures. Instead, they either thermally decompose into a mixture of their binary oxides (Bayer 1972; Strzelecki et al. 2021) or persist till melting (McMurdie and Hall 1947; Angapova and Serebrennikov 1973; Hikichi and Nomura 1987; Ushakov et al. 2001a; Kolitsch and Holtstam 2004; Shin et al. 2006; Rubatto and Hermann 2007; Wang et al. 2010; Ding et al. 2020; Ridley et al. 2022).

Thorite ($ThSiO_4$) is one oddity among the zircon structure materials. It undergoes a zircon → monazite transition at high temperatures (and also at high pressures) to the naturally occurring huttonite phase (Mumpton and Roy 1961; Finch et al. 1964; Taylor and Ewing 1978; Seydoux and Montel 1997; Mazeina et al. 2005; Shein et al. 2006; Harlov et al. 2007; Knyazev et al. 2017). According to work by Harlov et al. (2007), despite being a high temperature-high pressure phase relative to thorite, the monoclinic huttonite is demonstrated to be a lower temperature metastable phase when it is associated with REE monazites. As huttonite is ~7.8% denser than thorite, this thorite → huttonite transition contradicts the general observation that high-temperature polymorphs are the less dense phase (Taylor and Ewing 1978; Shein et al. 2006). The mechanism for such a transition has not been well explained, nor can it be easily explained by typical crystal-chemical arguments as noted above. Therefore, there is still research to be done to understand the crystal chemistry of thorium orthosilicates at elevated temperatures.

Response of zircon structure minerals to radiation. Many of the zircon structure-type minerals contain appreciable quantities of the naturally occurring radioactive elements U and Th.

Moreover, there are several zircon structure-types that contain essential radioactive elements (i.e., coffinite = $USiO_4$ and thorite = $ThSiO_4$). Thus, these structures experience radiation damage due to the accumulation of α-decay events over time (Anderson et al. 2017, 2019, 2020b, 2020a). To study these effects, the radiation dose can either be intrinsically created by doping the structure with a radionuclide (i.e., ^{238}Pu) (Boatner et al. 1984; Murakami et al. 1991; Weber 1993; Weber et al. 1994; Hanchar et al. 2003), or externally, by means of ion-beam irradiation (Weber et al. 1994; Meldrum et al. 1997b, 1999; Zhang et al. 2008b; Rafiuddin and Grosvenor 2015; Rafiuddin et al. 2020). Zircon structure-types under radiation may lose their long-range crystallinity and become aperiodic, the metamict state. The process of metamictization is reversible through thermal annealing of the long-range periodicity of the structure (Weber 1991; Geisler et al. 2005), although the short-range order of the structure may not be recovered, such as has been observed in irradiated pyrochlores (Weber et al. 1998). Metamict zircon-type materials experience softening in both elastic moduli and hardness and an increase in dissolution rate (Ewing et al. 1982). Several review papers have summarized the radiation effects on zircon structure-type materials from the structural and energetic (Ellsworth et al. 1994; Meldrum et al. 1997a, 2000; Ewing et al. 2003; Ewing 2007; Geisler et al. 2007; Weber and Ewing 2013; Beirau et al. 2016, 2017, 2018, 2019, 2021; Weber et al. 2019).

While damage of the zircon crystal structure in response to α-particle radiation is fairly well understood (Meldrum et al. 1997a, 2000; Ewing et al. 2003; Ewing 2007; Geisler et al. 2007; Weber and Ewing 2013; Beirau et al. 2017, 2018; Weber et al. 2019), incorporation of the Pb daughter product into the crystal structure is the subject of much debate, which has major implications on how geologic processes are dated (Watson et al. 1997; Kramers et al. 2009; Tanaka et al. 2010; Kogawa et al. 2012; Syverson et al. 2019). One of the major controversies concerns the oxidation of Pb, which can take the form of either Pb^{2+} or Pb^{4+} (Kramers et al. 2009; Tanaka et al. 2010; Kogawa et al. 2012; Syverson et al. 2019). From a crystallographic point of view, in an eightfold coordination environment, Pb^{4+} (0.94 Å) is similar in size to parent U^{4+} (1.00 Å) and Th^{4+} (1.05 Å), whereas Pb^{2+} (1.29 Å) is significantly larger (Shannon 1976). Additionally, if Pb^{4+} is the assumed oxidation state, then there is no need for charge balance by vacancies and P^{5+} for Si^{4+} substitution, which would be needed for Pb^{2+} (Kogawa et al. 2012; Syverson et al. 2019). However, the oxygen fugacity needed to allow for Pb^{4+} to be the stable oxidation state would be so oxidizing that U^{4+} would be oxidized to U^{6+}, making it unlikely to be incorporated into the zircon crystallographic lattice (Watson et al. 1997). Despite this observation, there are mixed results from X-ray absorption spectroscopy (XAFS) studies where both X-ray absorption near edge structure (XANES) and X-ray absorption fine structure (EXAFS) data indicate the presence of Pb^{2+} (Syverson et al. 2019), Pb^{4+} (Kramers et al. 2009), and mixed-valence Pb (Tanaka et al. 2010). Transmission electron microscopy also collaborates that the incorporation of Pb^{2+} in the crystal structure of zircon can be enhanced in P-rich systems by the xenotime-type, charge-coupled substitution ($Zr^{4+} + 2Si^{5+} = Pb^{2+} + 2P^{5+}$) (Kogawa et al. 2012). In a P-free system, without the above charge-balance reaction, most of the Pb is rejected from the zircon structure and instead is found to cluster as micro- to nanoscale $Pb^{2+}O$ domains residing preferentially in radiation-damaged areas of the zircon (Kogawa et al. 2012; Syverson et al. 2019).

Thermochemical properties of zircon structure compounds

The standard enthalpy of formation at 298 K (ΔH_f) of many compositional zircon-type material end-members has been determined. These are tabulated in Online Materials[1] Table S2 (Ellison and Navrotsky 1992; Ushakov et al. 2001a; Navrotsky and Ushakov 2005; Dorogova et al. 2007; Guo et al. 2015, 2016a; Strzelecki et al. 2020a). The values of ΔH_f that have yet to be determined are for the zircon-type end-members: behierite ($TaBO_4$), schiavinatoite ($NbBO_4$), rare earth orthochromates ($REECrO_4$), rare earth orthoarsenates ($REEAsO_4$), transuranium orthosilicates ($NpSiO_4$, $PuSiO_4$, and $AmSiO_4$), and thorium orthogermanate ($ThGeO_4$). These gaps offer opportunities for future thermodynamic research to be conducted on the determination of these values. One challenge for conducting such research is the availability of enough (approximately 10^1 to 10^3 mg) pure compounds for calorimetric or solubility measurements. For instance, all pure synthetic transuranium orthosilicates have been rarely synthesized (Keller 1963; Estevenon et al. 2020b, 2021a). For this reason, computational and empirical studies have been performed to fill the gaps in the experimental data, thus providing a basis for understanding the thermodynamics of some zircon-type materials. (Ferriss et al. 2010; Strzelecki et al. 2020b). So far, the only pure phase of $PuSiO_4$ has been synthesized by Keller (1963), and equally limited simulation work has been done with $PuSiO_4$ due to the complexity of dealing with 5*f* elements, in particular, the strong on-site Coulomb repulsion interaction of 5*f* electrons and relativistic effects, such as the scalar relativistic effect and spin-orbit coupling. Ferriss et al. (2010) used density functional theory to compute ΔH_f of $PuSiO_4$ at 0 K to be –1889.1 kJ/mol. A dense sampling grid of 0.07 $Å^{-1}$ and a high cut-off energy value of 800 eV were applied during the calculation to ensure precision and accuracy. However, for simplicity, the correction of on-site *f* electron interaction and relativistic effects were not considered in Ferriss et al. (2010). Further investigation using more accurate DFT methods may be needed, such as the DFT+*U* calculation with spin-orbit coupling taken into consideration. Strzelecki et al. (2020b) used empirical methods to derive ΔH_f at 298 K for $PuSiO_4$, $NpSiO_4$, and $AmSiO_4$ to be –1930.1 ± 4.1 kJ/mol, –1961.7 ± 4.1 kJ/mol, and –1802.0 ± 5.3 kJ/mol, respectively, which relied on the empirically determined relationship in isostructural ceramic materials (Sverjensky and Molling 1992) between the enthalpy of formation from the oxides ($\Delta H_{f,ox}$) and ionic radius of the metal cation (Navrotsky 2001). This, and derivatives of the method that use other parameters (i.e., ionic potentials or molar volumes), have been used in the derivation of other thermodynamic variables (Anderson and Anderson 1970; Sverjensky et al. 1997; Chen et al. 1999; Navrotsky 2001, 2005; Helean et al. 2003, 2004; Jenkins and Glasser 2003; Xu et al. 2010a; Qi et al. 2015; Guo et al. 2016b; Strzelecki et al. 2023).

We have modified and updated the figure reported in Strzelecki et al. (2020b), which shows variations in $\Delta H_{f,ox}$ of zircon structure materials as a function of the r_A/r_T (Fig. 4),

for which there is a negative linear correlation. From Figure 4, the HREE orthophosphates (e.g., xenotime and pretulite) are the most thermodynamically favored zircon structure-types with respect to their binary oxides ($PO_{2.5}$ and $HREEO_{1.5}$). It is therefore reasonable to assume that the orthoborate minerals, behierite ($TaBO_4$) and schiavinatoite ($NbBO_4$), should be the most energetically favorable zircon phases, with respect to the binary oxides [$BO_{1.5}$ and $(Nb,Ta)O_{2.5}$], as they exhibit the largest values of r_A/r_T. However, such predictions do not fully justify the natural rarity of behierite and schiavinatoite, as Nb, Ta, and B are all incompatible elements that are enriched in felsic magmas (Parker and Fleischer 1968; Leeman and Sisson 1996; Schulz and Papp 2014). Instead, the rarity of these two phases is more easily explained by the formation of Nb and Ta anionic complexes in the melt. This leads to oxide minerals, such as tantalite [$(Fe,Mn)Ta_2O_6$] and columbite [$(Fe,Mn)Nb_2O_6$], which may be more thermodynamically favorable than the behierite and schiavinatoite counterparts (Parker and Fleischer 1968; Schulz and Papp 2014).

Notably, all *f*-block orthosilicates (excluding zircon and hafnon) are outliers in Figure 4, which do not follow the linear trend of all other zircon-structure materials. From this perspective, it can be thought that *f*-block orthosilicates, due to both the relatively large A-site cations and T-site cation (Si), have no ideal ratio of r_A/r_T for a stable zircon structure. Large MO_8 dodecahedra may not be effectively compensated by smaller SiO_4 tetrahedra, and overall this leads to the destabilization of the structure. Such an argument is well reflected by their low endothermic enthalpies of formation. This also suggests, using an empirical model, that ionic interactions in the zircon structure may not be sufficient to capture the energetic landscape of *f*-block zircon-structure materials where partial covalency has been demonstrated (Vitova et al. 2017; Su et al. 2020; Marcial et al. 2021).

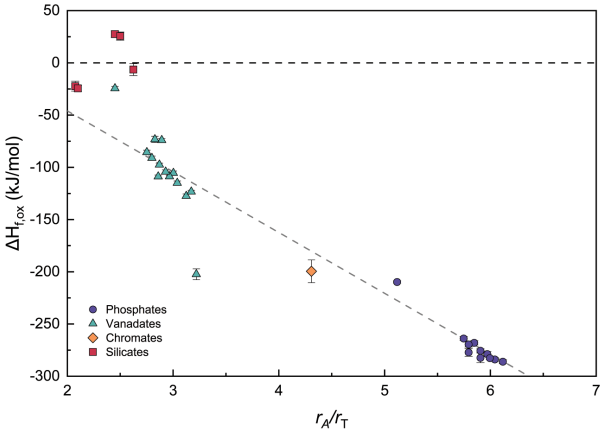

Figure 4. Enthalpy of formation from binary oxides, obtained for orthosilicates ($ASiO_4$) (Langmuir 1978; Langmuir and Chatham 1980; Ellison and Navrotsky 1992; Grenthe et al. 1993; Mazeina et al. 2005; Navrotsky and Ushakov 2005; Szenknect et al. 2013; Guo et al. 2015, 2016a; Strzelecki et al. 2020b), orthochromates ($ACrO_4$) (Lee and Nassaralla 2006), orthovanadates (AVO_4) (Dorogova et al. 2007), and orthophosphates (APO_4) (Marinova et al. 1973; Ushakov et al. 2001a; Strzelecki et al. 2022) that crystallize with the zircon structure ($I4_1/amd$) as a function of r_A/r_T. The equation describing the gray dashed line is $\Delta H_{f,ox}$(kJ/mol) = [–58.2(±1.4)·(r_A/r_T)] + [70.5(±6.4)], which has an adjusted R^2 value of 0.99. The details describing the regression are supplied in the main text. (Color online.)

The other outlier is $CeVO_4$ from the work of Dorogova et al. (2007). The root reason for such an outlier was not discussed in their study. Nevertheless, it is possible that this outlier value may be due to the partial oxidation of Ce^{3+} to Ce^{4+} before the calorimetric measurements were made, which might have led to a less exothermic enthalpy value (Helean and Navrotsky 2002; Guo et al. 2014).

If one removes these outliers, a linear regression on the remaining values results in the following linear relationship:

$$\Delta H_{f,ox}(\text{kJ/mol}) = [-58.2(\pm1.4)\cdot(r_A/r_T)] + [70.5(\pm6.4)] \quad (1)$$

with an adjusted $R^2 = 0.99$. This linear correlation between $\Delta H_{f,ox}$ and r_A/r_T can be used as an empirical relation for predicting the enthalpies of formation of other zircon-structure materials, including behierite ($TaBO_4$), schiavinatoite ($NbBO_4$), rare earth orthochromates ($REECrO_4$), and rare earth orthoarsenates ($REEAsO_4$). Lastly, the enthalpy value of binary oxides used for deriving the $\Delta H_{f,ox}$ values were taken from: Chase (1998), for $TaO_{2.5}$ and $NbO_{2.5}$; Konings et al. (2014) for all the lanthanide oxides ($LnO_{1.5}$); Morss et al. (1993) for $YO_{1.5}$; Ushakov et al. (2001a) for $ScO_{1.5}$; and Robie and Hemingway (1995) for $AsO_{1.5}$, $BO_{1.5}$, and $CrO_{1.5}$. These values are tabulated in Online Materials[1] Table S2.

Natural zircon-structure minerals dominantly exist as continuous solid solutions with substitutions occurring in both the A- and T-sites. In comparison to the thermodynamics of the end-members, there has been much less systematic work examining the thermodynamics of mixing for various metal cations that can be quantified by an enthalpy of mixing (ΔH_{mix}). To date, there are only limited measurements ΔH_{mix} values for zircon-structure materials (Guo et al. 2016a; Marcial et al. 2021; Shelyug et al. 2021; Strzelecki et al. 2022) and computational studies (Mogilevsky 2007; Ji et al. 2019; Migdisov et al. 2019). The findings suggest that ideal cation mixing in the zircon structure is not always correct and can have significant impacts on phase stability. Here, we emphasize that non-ideal mixing in zircon can be used to engineer more stable waste form ceramics or high-temperature thermal barrier coating (TBC) materials. Thus, the thermodynamics of mixing in the zircon structure deserves more research. For instance, the uranothorite solid solution in which U and Th occur is a system that exemplifies a strong nonideal mixing effect (Guo et al. 2016a; Marcial et al. 2021). The work of Marcial et al. (2021) suggests that the nonideal mixing effect from U and Th in the cationic sublattice, characterized by a subregular solution model: $\Delta H_{mix} = [w_{12}(1 - x) + w_{21}x]x(1 - x)$, where w_{12} and w_{21} are the asymmetric interaction parameters and x is the mole fraction of one of the constituents being mixed, can create significantly extended stability fields, both in temperature and oxygen fugacity, for forming uranothorite with high U contents at conditions where pure coffinite is unstable. The authors attributed the non-ideal mixing effect to a covalency-driven electron transfer mechanism (Marcial et al. 2021), which may also play a role in mixing other *f*-block elements (i.e., Pu) in the zircon structure. Future experimental work on $PuSiO_4$ and associated solid solutions may help to confirm this hypothesis.

Stabilization from a possible negative enthalpy of mixing may help the stabilization of Pu (or Am) in the zircon matrix for long-term use as an actinide waste form (Marcial et al. 2021). There are also future research opportunities to investigate the mixing of multiple elements in the A- and T-sites, so that one can evaluate entropic contributions in high entropy zircon ceramics for potentially improved phase stability.

Heat capacity (C_P), standard entropy ($S°$), and Gibbs Free Energy (ΔG) of zircon structure compounds

In comparison to the experimental studies devoted to determining the ΔH_f of zircon structured materials, significantly less work has been done in determining the isobaric heat capacity (C_P), standard entropy ($S°$), or free energy (ΔG) of these materials. One reason for the lack of experimental derivations for $S°$, is that the C_P must be determined below 10 K. Conventionally, this has been done by means of adiabatic calorimetry, which requires relatively large amounts of sample (1–10 g) and significant amounts of time, which ultimately has led to the lack of these measurements (Navrotsky 1994). Nonetheless, the values of $S°$ for rare earth orthophosphates and rare earth orthovanadates are known from adiabatic calorimetric measurements, which are tabulated in Online Materials[1] Table S3 (Gavrichev et al. 2006, 2010a, 2010b, 2010c, 2011, 2012a, 2012b, 2013b, 2014; Ryumin et al. 2017; Tyurin et al. 2020). Besides experimental approaches, the DFT method can be used to study heat capacity and entropy by computing phonon normal modes with tunable external perturbations (e.g., temperature and pressure). In the work of Marcial et al. (2021) a comparison of theoretical heat capacity and empirical heat capacity values of $USiO_4$ and $ThSiO_4$ was performed (Online Materials[1] Fig. S3). A discussion of entropy values of $USiO_4$ was also given by Konings and Plyasunov (2017).

On the other hand, $S°$ may be derived from an empirical relation with the molar volume (V_m) of a compound (Jenkins and Glasser 2003; Glasser 2011). The linear equations presented by Jenkins and Glasser (2003) have been successfully used to calculate various unknown $S°_{298K}$ values (Guo and Xu 2017; Strzelecki et al. 2020a, 2023; Goncharov et al. 2022). However, recent work of Strzelecki et al. (2022) noticed large discrepancies between the extrapolated $S°_{298K}$ values based the method of Jenkins and Glasser (2003) for phosphate minerals and experimentally determined values (Robie and Hemingway 1995; Navrotsky et al. 2015; Gysi et al. 2016; Gysi and Harlov 2021; Migdisov et al. 2016; Van Hoozen et al. 2020). A new set of empirical $S°_{298K} - V_m$ linear equations was thus proposed by Strzelecki et al. (2022) to include phosphate minerals and further extended to all minerals. Lastly, knowing both the ΔG_f and ΔH_f values for a given material, an indirect method for determining the $S°$ value is to calculate ΔS_f through rearrangement of the Gibbs free energy equation ($\Delta G_f = \Delta H_f - T\Delta S_f$) and then to access the $S°$ value for a given compound.

Using the indirect method for determining $S°$, one is assuming that both ΔG_f and ΔH_f are known. While this is a safe assumption for ΔH_f, there are many gaps in our knowledge of experimental measurements of ΔG_f. Even so, solubility studies have been conducted on nearly all zircon-structured orthosilicate minerals (Schuiling et al. 1976; Newton et al. 2005; Szenknect et al. 2016) and several of the compositional end-members of xenotime to derive the ΔG_f values (Gysi et al. 2015, 2016; Gysi and Harlov 2021). Adiabatic calorimetry papers (Gavrichev et al. 2006, 2010a, 2010b, 2010c, 2011, 2012a, 2012b, 2013b, 2014; Ryumin et al. 2017; Tyurin et al. 2020) also report ΔG_f values, which were calculated from the measured ΔH_f values (Ushakov et al. 2001a; Dorogova et al. 2007) in conjunction with the values of $S°$. We tabulated the values of ΔG_f for zircon structure phases in Online Materials[1] Table S4. As discussed above, it is useful to study how mixing impacts the thermodynamics of zircon structure-type materials. If the mixing is ideal, then the entropy of mixing (ΔS_{mix}) can be calculated by using the Boltzmann entropy formula:

$$\Delta S_{mix,config} = -R\cdot[(1-x)\cdot\ln(1-x) + x\cdot\ln(x)] \quad (2)$$

Unlike ΔH_{mix}, there have been no experimental studies of the free energy of mixing (ΔG_{mix}) in the zircon structure.

Thermophysical parameters of zircon structure compounds

Thermal expansivity (α), also referred to as the coefficient of thermal expansion (CTE), and isothermal compressibility (β) are important thermodynamic parameters for the equation of states that describe how a given crystal structure will respond to temperature or pressure. Thermal expansivity (α) and compressibility (β) are defined by:

$$\alpha = V^{-1}(\partial V/\partial T)_P. \quad (3)$$
$$\beta = -V^{-1}(\partial V/\partial P)_T. \quad (4)$$

The following equations demonstrate the volume expansion or volume compressibility, which are important as they are also linked to the isobaric (C_P) and isochoric (C_v) heat capacities, as given in the following equation:

$$C_P - C_v = TV\alpha^2/\beta. \quad (5)$$

However, one can also create a one-dimensional form of expansivity or compressibility to derive either linear thermal expansivity or linear compressibility (Xu et al. 2010a, 2010b).

Most zircon-type structure compounds respond to temperature or pressure anisotropically in that the expansion or contraction of the *a*- and *c*-axis are not equivalent. When a zircon-structure material undergoes thermal expansion, the *c*-axis tends to expand more than the *a*-axis (Bayer 1972; Subbarao et al. 1990; Mursic et al. 1992; Varghese et al. 2015; Beirau et al. 2016; Knyazev et al. 2017; Ding et al. 2020). However, when a zircon-type structure material is compressed, the *c*-axis contracts less than the *a*-axis. The reason for the anisotropic behavior of both thermal expansion and compressibility is largely the same and can be explained by collective motions/distortions of TO_4 tetrahedra and MO_8 dodecahedra (Fig. 1). MO_8 dodecahedra provide more flexibility along the *a*-axis due to the higher freedom of corner-sharing $MO2_4$ tetrahedra. These latter can relax the structure during expansion and result in a smaller change along the *a*-axis compared to the *c*-axis. Consequently, due to

the higher repulsion experienced by edge-sharing compared to corner-sharing, the *c*-axis expands more than the *a*-axis. As thermal expansion is the reverse of baric compression, the reason for the c-axis contracting less than the *a*-axis can be explained by the same process. Here, the zircon structure is more flexible along the *a*-axis due to the higher freedom of corner-sharing $MO2_4$ tetrahedra during compression, which results in a greater change along the *a*-axis compared to the *c*-axis, along which the TO_4 is more incompressible (Li et al. 2007; Marcial et al. 2021). Consequently, due to the higher repulsion arising from the edge-sharing over corner-sharing, the *c*-axis contracts less than the *a*-axis.

Thermal expansivity (α) of zircon structure compounds

There are three main methods for deriving the coefficient of thermal expansion. These methods include dilatometry, interferometry, and in situ high-temperature X-ray and neutron diffraction techniques (Newnham 2005). Many of the α values of the compositional end-members for zircon structure materials have been tabulated in the literature by means of one, or more, of these three techniques (Online Materials[1] Table S5) (Bayer 1972; Subbarao et al. 1990; Strzelecki et al. 2021). It is of more interest to be able to relate these parameters to the underlying crystal chemistry of the materials to systematically predict structure and properties relationships (Navrotsky 1994). As stated above, many thermodynamic variables of isostructural inorganic materials are able to be studied through the existence of different, empirically derived relationships (Anderson and Anderson 1970; Sverjensky et al. 1997; Chen et al. 1999; Navrotsky 2001, 2005; Helean et al. 2003, 2004; Xu et al. 2010a; Qi et al. 2015; Guo et al. 2016b). These empirically derived relationships link specific thermodynamic variables to the varying component of the isostructural materials and allow for study of the periodicity of a particular variable.

Megaw (1973) argues that α is inversely proportional to the Pauling bond strength (PBS), which is defined as the cation valence divided by its coordination number. Newnham (2005) shows that bond strength is approximately proportional to $\alpha^{-1/2}$. Each of these arguments is based on strong interatomic forces, which are commonly correlated with low thermal expansion, whereas weak interatomic forces are commonly correlated with high thermal expansion. If we apply this to zircon structure materials by calculating the PBS for the A-site metal cations (Fig. 5a), we see that there are two trends that emerge. The first trend is that there is a proportionality between the PBS of the A-site metal cation to $\alpha^{-1/2}$ across all zircon-structure materials. This is validated by the fact that $CaCrO_4$ (PBS = 0.25) has the highest value of α (Bayer 1972), while $TaBO_4$ (PBS = 0.625) has the lowest α value (Bayer 1972). Such an observation demonstrates that $CaCrO_4$ has weaker interatomic forces than $TaBO_4$. The second trend is that when PBS is equal, the trend will show which materials within a given zircon-structure subgroup have the greatest interatomic forces. This is supported by the observation that $ThSiO_4$ has the smallest value of α (Subbarao et al. 1990; Knyazev et al. 2017), whereas $CeSiO_4$ exhibits the highest one (Strzelecki et al. 2021). This could also be due to their overall thermodynamic stabilities, as discussed above.

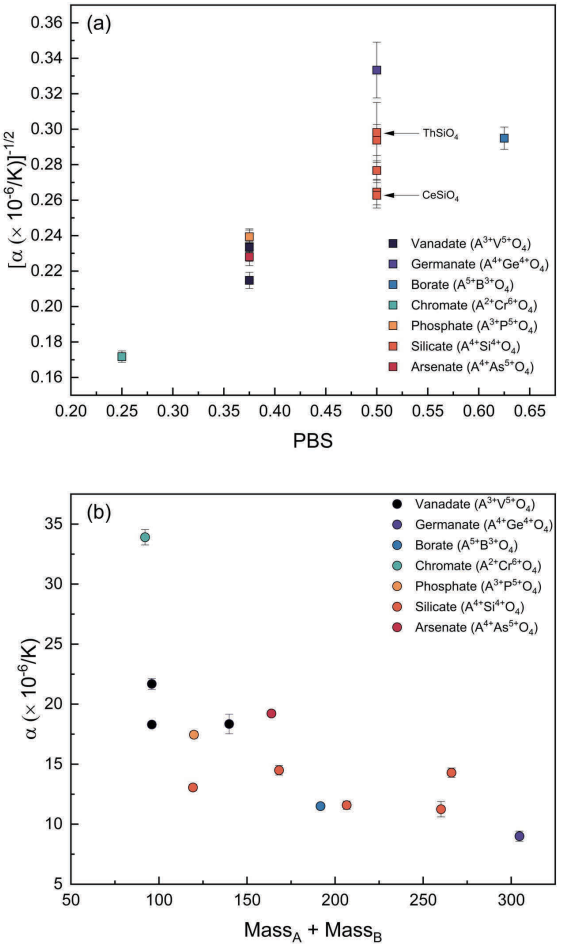

Figure 5. (**a**) Comparison of the negative cubed root of the thermal expansion coefficient ($\alpha^{-1/2}$) of various zircon-type materials as a function of the Pauling bond strength (PBS) of the A-site metal cation, where PBS was calculated by taking the charge of the A-site metal cation divided by its coordination number (CN = 8). (**b**) α of the various zircon-type materials as a function of the sum of the mass of the A- and B-site cations (Bayer 1972; Subbarao et al. 1990; Mursic et al. 1992; Varghese et al. 2015; Knyazev et al. 2017; Ding et al. 2020; Strzelecki et al. 2021). (Color online.)

Furthermore, Subbarao et al. (1990) and Strzelecki et al. (2021) studied CTEs of zircon-type phases by correlating them to the sum of the atomic weights of the A-site and B-site cations (Fig. 5b) (Bayer 1972; Subbarao et al. 1990; Mursic et al. 1992; Varghese et al. 2015; Knyazev et al. 2017; Ding et al. 2020). The CTEs of the $M^{4+}T^{4+}O_4$ zircon-type phases decrease with an increasing in the overall mass of the A and B site cations. While a similar trend is also seen when using PBS, here Hooke's law is expressed as the heaviest combined masses expand at the slowest rate.

Compressibility (β) of zircon structure compounds

There are several methods for studying the compressibility of a given material, including resonant ultrasonic spectroscopy (Balakirev et al. 2019; Goncharov et al. 2021), nanoindentation

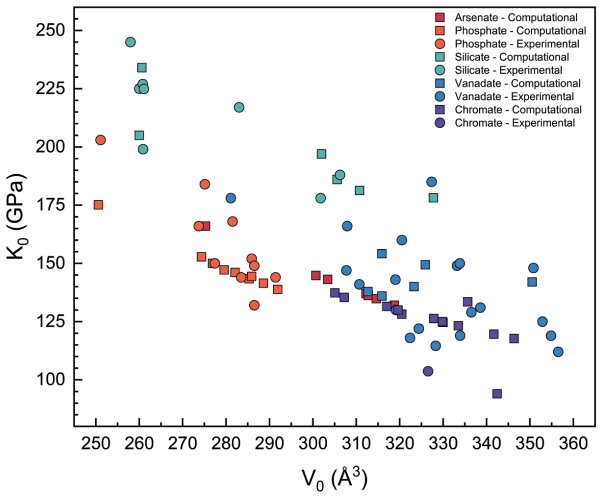

Figure 6. Comparison of bulk moduli vs. volume for all zircon-type orthosilicates. Circle symbols denote those values derived by experimental methods, while squares symbols denote computational derived values (Armbruster 1976; Hazen and Finger 1979; Crocombette and Ghaleb 1998; Yukiko Hirano et al. 2002; Ono et al. 2004a; Van Westrenen et al. 2004; Wang et al. 2004; Li et al. 2006, 2009, 2011, 2014; Long et al. 2006; Mogilevsky et al. 2006; Bose et al. 2008, 2009; Errandonea and Manjón 2008; Zhang et al. 2008a; Errandonea et al. 2009b, 2011, 2014; Garg et al. 2009, 2013, 2014; Zhang et al. 2009; Lacomba-Perales et al. 2010; López-Solano et al. 2010; Huang et al. 2012a; Bauer et al. 2014; Paszkowicz et al. 2014; Garg and Errandonea 2015; Popescu et al. 2016; Yue et al. 2016; Gomis et al. 2017; Errandonea and Garg 2018; Mondal et al. 2020; Ehlers et al. 2022; Strzelecki et al. 2023). (Color online.)

(Beirau et al. 2021), and in situ high-pressure X-ray and neutron diffraction techniques (Anderson 1984, 1995, 2007; Navrotsky 1994). Many of the β values for the compositional end-members for zircon-structure materials have been tabulated in the literature through at least one of these three techniques, if not a combination of several. However, these literature values are commonly reported as the inverse of compressibility (1/β), which is referred to as the bulk modulus (K). We have tabulated the values of K for several zircon-structured materials in Online Materials[1] Table S6. It is again interesting to examine broadly the structure-property relationships of all zircon-structure materials to gain knowledge of the underlying crystal chemistry and to systematically predict relationships between structure and properties. Here, there is an empirical relationship between K and its inverse proportionality to zero-point pressure volumes (V_0) of isostructural inorganic materials, in that larger unit-cell volumes are generally more compressible and thus have a smaller bulk modulus (Anderson and Anderson 1970; Xu et al. 2010a).

In Figure 6, K vs. V_0 is plotted for all the available zircon-structured materials (orthosilicates, orthophosphates, and orthovanadate) (Armbruster 1976; Hazen and Finger 1979; Crocombette and Ghaleb 1998; Hirano et al. 2002a; Ono et al. 2004a; Van Westrenen et al. 2004; Wang et al. 2004; Li et al. 2006, 2009, 2011, 2014; Long et al. 2006; Mogilevsky et al. 2006; Bose et al. 2008, 2009; Errandonea and Manjón 2008; Zhang et al. 2008a; Errandonea et al. 2009b, 2011, 2014; Garg et al. 2009, 2013, 2014; Zhang et al. 2009; Lacomba-Perales et al. 2010; López-Solano et al. 2010; Huang et al. 2012a; Bauer et al. 2014; Paszkowicz et al. 2014; Garg and Errandonea 2015; Popescu et al. 2016; Yue et al. 2016; Gomis et al. 2017; Errandonea and Garg 2018; Mondal et al. 2020; Ehlers et al. 2022; Strzelecki et al. 2023). It is worth noting that the two orthoborate minerals are missing from this figure. When comparing the available data for the three different zircon structure-types, the MO_8 unit is largely unchanged from orthophosphate to orthovanadate, but rather, the change is in the different TO_4 units from which these classes got their names. Through this, one can see how incompressible the silicate tetrahedron, with the highest of the bulk moduli, is even when comparing similar overall unit-cell sizes (i.e., $CeSiO_4$, $TbPO_4$, $GdVO_4$).

Implications

In this review, we evaluated recent advances in the crystal chemistry and thermodynamic properties of zircon structure-type materials. We focused on empirically derived structure-property relationships, which can be used to obtain thermodynamic functions and support their potential applications in the design and improvement of a compositionally diverse class of materials. In addition, we have identified several key gaps in the thermodynamics for several zircon structure-type minerals and critical needs in the understanding of how cation mixing at the A- and/or T-site affects thermodynamics parameters. These gaps can be viewed as the starting point for future research in furthering our understanding of the zircon-structure minerals and ceramics. This up-to-date summary of knowledge of zircon-type materials should help researchers continue developing a fundamental understanding of their mineral chemistry. It should also help to promote the use of zircon-type materials for applications in industry, such as in actinide waste disposal and in aeronautical engineering as environmental and thermal barrier coatings.

Funding

We acknowledge the supports by the National Science Foundation (NSF), Division of Earth Sciences, under award no. 2149848, and Division of Materials Research, under award no. 2144792.

Dedication

We dedicate this work to Alexandra Navrotsky, a pioneer in mineral thermochemistry, on the occasion of her 80th birthday.

References cited

Achary, S.N., Patwe, S.J., Krishna, P.S.R., Sindhe, A.B., and Tyagi, A.K. (2007) Crystal structure analysis of scheelite and zircon type thorium germanates: A neutron diffraction study. Journal of Alloys and Compounds, 438, 274–278, https://doi.org/10.1016/j.jallcom.2006.08.025.

Anderson, O.L. (1984) A universal thermal equation-of-state. Journal of Geodynamics, 1, 185–214, https://doi.org/10.1016/0264-3707(84)90027-9.

——— (1995) Equations of State of Solids for Geophysics and Ceramic Science, 432 p. In H. Charnock, J.F. Dewey, S.C. Morris, A. Navrotsky, E.R. Oxburgh, R.A. Price, and B.J. Skinner, Eds., Oxide Monographs on Geology and Geophysics, vol. 31. Oxford University Press.

Anderson, D.L. (2007) Elasticity and solid-state geophysics. In New Theory of the Earth, p. 233–245. Cambridge University Press.

Anderson, D.L. and Anderson, O.L. (1970) The bulk modulus-volume relationship for oxides. Journal of Geophysical Research, 75, 3494–3500, https://doi.org/10.1029/JB075i017p03494.

Anderson, A.J., Hodges, K., and van Soest, M.C. (2017) Empirical constraints on the effects of radiation damage on helium diffusion in zircon. Geochimica et Cosmochimica Acta, 218, 308–322, https://doi.org/10.1016/j.gca.2017.09.006.

Anderson, A.J., Hodges, K., van Soest, M.C., and Hanchar, J.M. (2019) Helium diffusion in natural xenotime. Geochemistry, Geophysics, Geosystems, 20, 417–433, https://

doi.org/10.1029/2018GC007849.
Anderson, A.J., van Soest, M.C., Hodges, K., and Hanchar, J.M. (2020a) Helium diffusion in zircon: Effects of anisotropy and radiation damage revealed by laser depth profiling. Geochimica et Cosmochimica Acta, 274, 45–62, https://doi.org/10.1016/j.gca.2020.01.049.
Anderson, A.J., Hanchar, J.M., Hodges, K., and van Soest, M.C. (2020b) Mapping radiation damage zoning in zircon using Raman spectroscopy: Implications for zircon chronology. Chemical Geology, 538, 119494, https://doi.org/10.1016/j.chemgeo.2020.119494.
Angapova, L.E. and Serebrennikov, V.V. (1973) Thermal stability of rare earth arsenates. Zhurnal Neorganicheskoj Khimii, 18, 1706–1708.
Armbruster, A. (1976) Infrared reflection studies on the phosphates, arsenates and vanadates of lutetium and yttrium. Journal of Physics and Chemistry of Solids, 37, 321–327, https://doi.org/10.1016/0022-3697(76)90094-9.
Balakirev, F.F., Ennaceur, S.M., Migliori, R.J., Maiorov, B., and Migliori, A. (2019) Resonant ultrasound spectroscopy: The essential toolbox. The Review of Scientific Instruments, 90, 121401, https://doi.org/10.1063/1.5123165.
Bandiello, E., Errandonea, D., González-Platas, J., Rodríguez-Hernández, P., Muñoz, A., Bettinelli, M., and Popescu, C. (2020) Phase behavior of $TmVO_4$ under hydrostatic compression: An experimental and theoretical study. Inorganic Chemistry, 59, 4882–4894, https://doi.org/10.1021/acs.inorgchem.0c00147.
Bastide, J.P. (1987) Systématique simplifiée des composés ABX_4 ($X = O^{2-}, F^-$) et evolution possible de leurs structures cristallines sous pression. Journal of Solid State Chemistry, 71, 115–120, https://doi.org/10.1016/0022-4596(87)90149-6.
Baudracco-Gritti, C., Quartieri, S., Vezzalini, G., Permingeat, F., Pillard, F., and Rinaldi, R. (1987) Une wakefieldite- (Ce) non plombifère: Nouvelles données sur l'espèce minérale correspondant à l'orthovanadate de cérium. Bulletin de Minéralogie (Paris), 110, 657–663, https://doi.org/10.3406/bulmi.1987.8010.
Bauer, J.D., Labs, S., Weiss, S., Bayarjargal, L., Morgenroth, W., Milman, V., Perlov, A., Curtius, H., Bosbach, D., Zänker, H., and others. (2014) High-pressure phase transition of coffinite, $USiO_4$. The Journal of Physical Chemistry C, 118, 25141–25149, https://doi.org/10.1021/jp506368q.
Bayer, G. (1972) Thermal expansion of ABO_4-compounds with zircon- and scheelite structures. Journal of the Less Common Metals, 26, 255–262, https://doi.org/10.1016/0022-5088(72)90045-8.
Begun, G.M., Beall, G.W., Boatner, L.A., and Gregor, W.J. (1981) Raman spectra of the rare earth orthophosphates. Journal of Raman Spectroscopy, 11, 273–278, https://doi.org/10.1002/jrs.1250110411.
Beirau, T., Nix, W.D., Bismayer, U., Boatner, L.A., Isaacson, S.G., and Ewing, R.C. (2016) Anisotropic mechanical properties of zircon and the effect of radiation. Physics and Chemistry of Minerals, 43, 627–638, https://doi.org/10.1007/s00269-016-0822-9.
Beirau, T., Nix, W.D., Pöllmann, H., and Ewing, R.C. (2017) Radiation-induced effects on the mechanical properties of natural $ZrSiO_4$: Double cascade-overlap damage accumulation. Physics and Chemistry of Minerals, 45, 435-442, https://doi.org/10.1007/s00269-017-0931-0.
Beirau, T., Nix, W.D., Ewing, R.C., Pöllmann, H., and Saljet, E.K.H. (2018) Radiation-damage-induced transitions in zircon: Percolation theory applied to hardness and elastic moduli as a function of density. Applied Physics Letters, 112, 201901, https://doi.org/10.1063/1.5030626.
Beirau, T., Oliver, W.C., Reissner, C.E., Nix, W.D., Pöllmann, H., and Ewing, R.C. (2019) Radiation-damage in multi-layered zircon: Mechanical properties. Applied Physics Letters, 115, 081902, https://doi.org/10.1063/1.5119207.
Beirau, T., Rossi, E., Sebastiani, M., Oliver, W.C., Pöllmann, H., and Ewing, R.C. (2021) Fracture toughness of radiation-damaged zircon studied by nanoindentation pillar-splitting. Applied Physics Letters, 119, 231903, https://doi.org/10.1063/5.0070597.
Bernhard, F., Walter, F., Ettinger, K., Taucher, J., and Mereiter, K. (1998) Pretulite, $ScPO_4$, a new scandium mineral from the Styrian and Lower Austrian lazulite occurrences, Austria. American Mineralogist, 83, 625–630, https://doi.org/10.2138/am-1998-5-622.
Berzelius, J.J. (1829) Untersuchung eines neuen Minerals und einer darin enthaltenen zuvor unbekannten Erde. Annalen der Physik und Chemie, 385–415.
Boatner, L.A. (2002) Synthesis, structure, and properties of monazite, pretulite, and xenotime. Reviews in Mineralogy and Geochemistry, 48, 87–121.
Boatner, L.A., Beall, G.W., Abraham, M.M., Finch, C.B., Huray, P.G., and Rappaz, M. (1980) Monazite and other lanthanide orthophosphates as alternate actinide waste forms. In Scientific Basis for Radioactive Waste Management, 289–296. Springer.
Boatner, L.A., Abraham, M.M., and Sales, B.C. (1984) Lanthanide orthophosphate ceramics for the disposal of actinide-contaminated nuclear wastes. Inorganica Chimica Acta, 94, 146–148, https://doi.org/10.1016/S0020-1693(00)94610-3.
Bose, P.P., Mittal, R., Choudhury, N., and Chaplot, S.L. (2008) Inelastic neutron scattering and lattice dynamics of ZrO, Y_2O_3, and $ThSiO_4$. Pramana, 71, 1141–1146, https://doi.org/10.1007/s12043-008-0237-3
Bose, P.P., Mittal, R., and Chaplot, S.L. (2009) Lattice dynamics and high pressure phase stability of zircon structured natural silicates. Physical Review B: Condensed Matter and Materials Physics, 79, 1–8, https://doi.org/10.1103/PhysRevB.79.174301.
Bowring, S.A. and Schmitz, M.D. (2003) High-precision U-Pb zircon geochronology and the stratigraphic record. In J.M. Hanchar and P.W.O. Hoskin, Eds., Zircon, 53, 305–326. Reviews in Mineralogy and Geochemistry, Mineralogical Society of America, Chantilly, Virginia.
Buck, H.M., Cooper, M.A., Černý, P., Grice, J.D., and Hawthorne, F.C. (1999) Xenotime-(Yb), $YbPO_4$, a new mineral species from the Shatford Lake pegmatite group, southeastern Manitoba, Canada. Canadian Mineralogist, 37, 1303–1306.
Buerger, M.J. (1961) Polymorphism and phase transformations. Fortschritte der Mineralogie, 9.
Burnham, A.D. and Berry, A.J. (2012) An experimental study of trace element partitioning between zircon and melt as a function of oxygen fugacity. Geochimica et Cosmochimica Acta, 95, 196–212, https://doi.org/10.1016/j.gca.2012.07.034.
Burns, P.C., Ewing, R.C., and Navrotsky, A. (2012) Nuclear fuel in a reactor accident. Science, 335, 1184–1188, https://doi.org/10.1126/science.1211285.
Chakoumakos, B.C., Abraham, M.M., and Boatner, L.A. (1994) Crystal structure refinements of zircon-type MVO_4 (M = Sc, Y, Ce, Pr, Nd, Tb, Ho, Er, Tm, Yb, Lu). Journal of Solid State Chemistry.
Chase, M.W.J. (1998) NIST-JANAF thermochemical tables, fourth edition. Journal of Physical and Chemical Reference Data, 9.
Chen, F., Ewing, R.C., and Clark, S.B. (1999) The Gibbs free energies and enthalpies of formation of U^{6+} phases: An empirical method of prediction. American Mineralogist, 84, 650–664, https://doi.org/10.2138/am-1999-0418.
Cherniak, D.J. and Watson, E.B. (2003) Diffusion in zircon. In J.M. Hanchar and P.W.O. Hoskin, Eds., Zircon, 53, 113–144. Reviews in Mineralogy and Geochemistry, Mineralogical Society of America, Chantilly, Virginia.
Clavier, N., Podor, R., and Dacheux, N. (2011) Crystal chemistry of the monazite structure. Journal of the European Ceramic Society, 31, 941–976, https://doi.org/10.1016/j.jeurceramsoc.2010.12.019.
Clavier, N., Mesbah, A., Szenknect, S., and Dacheux, N. (2018) Monazite, rhabdophane, xenotime and churchite: Vibrational spectroscopy of gadolinium phosphate polymorphs. Spectrochimica Acta. Part A: Molecular and Biomolecular Spectroscopy, 205, 85–94, https://doi.org/10.1016/j.saa.2018.07.016.
Climent, E., Gallardo, J.M., de Paz, J.R., Taira, N., and Puche, R.S. (2009) Phase transition induced by pressure in $TbCrO_4$ oxide: Relationship structure-properties. Journal of Alloys and Compounds, 488, 524–527, https://doi.org/10.1016/j.jallcom.2008.10.060.
Climent-Pascual, E., Romero de Paz, J., Gallardo-Amores, J.M., and Sáez-Puche, R. (2007) Ferromagnetism vs. antiferromagnetism of the dimorphic $HoCrO_4$ oxide. Solid State Sciences, 9, 574–579.
Corfu, F., Hanchar, J.M., Hoskin, P.W.O., and Kinny, P. (2003) Atlas of zircon textures. In J.M. Hanchar and P.W.O. Hoskin, Eds., Zircon, 53, 469–500. Reviews in Mineralogy and Geochemistry, Mineralogical Society of America, Chantilly, Virginia.
Costin, D.T., Mesbah, A., Clavier, N., Dacheux, N., Poinssot, C., Szenknect, S., and Ravaux, J. (2011) How to explain the difficulties in the coffinite synthesis from the study of uranothorite? Inorganic Chemistry, 50, 11117–11126, https://doi.org/10.1021/ic2016758.
Crocombette, J.P. and Ghaleb, D. (1998) Modeling the structure of zircon ($ZrSiO_4$): Empirical potentials, ab initio electronic structure. Journal of Nuclear Materials, 257, 282–286, https://doi.org/10.1016/S0022-3115(98)00454-1.
Curtis, C.E., Doney, L.M., and Johnson, J.R. (1954) Some properties of hafnium oxide, hafnium silicate, calcium hafnate, and hafnium carbide. Journal of the American Ceramic Society, 37, 458–465, https://doi.org/10.1111/j.1151-2916.1954.tb13977.x.
Darnley, A.G., English, T.H., Sprake, O., Preece, E.R., and Avery, D. (1965) Ages of uraninite and Coffinite from south-west England. Mineralogical Magazine and Journal of the Mineralogical Society, 34, 159–176, https://doi.org/10.1180/minmag.1965.034.268.13.
Davis, D.W., Williams, I.S., and Krogh, T.E. (2003) Historical development of zircon geochronology. In J.M. Hanchar and P.W.O. Hoskin, Eds., Zircon, 53, 145–182. Reviews in Mineralogy and Geochemistry, Mineralogical Society of America, Chantilly, Virginia.
Deliens, M. and Piret, P. (1986) La kusuïte devient la wakefieldite-(Ce) plombifère. Bulletin de Minéralogie (Paris), 109, 305, https://doi.org/10.3406/bulmi.1986.7938.
Demartin, F., Diella, V., Gramaccioli, C.M., and Pezzotta, F. (2001) Schiavinatoite, $(Nb,Ta)BO_4$, the Nb analogue of behierite. European Journal of Mineralogy, 13, 159–165, https://doi.org/10.1127/0935-1221/01/0013-0159.
Denton, A.R. and Ashcroft, N.W. (1991) Vegard's law. Physical Review A, 43, 3161–3164, https://doi.org/10.1103/PhysRevA.43.3161.
Ding, Z., Ridley, M., Deijkers, J., Liu, N., Hoque, M.S., Gaskins, J., Zebarjadi, M., Hopkins, P.E., Wadley, H., Opila, E., and others. (2020) The thermal and mechanical properties of hafnium orthosilicate: Experiments and first-principles calculations. Materialia, 12, 100793, https://doi.org/10.1016/j.mtla.2020.100793.
Dong, X., Oganov, A.R., Cui, H., Zhou, X.F., and Wang, H.T. (2022) Electronegativity and chemical hardness of elements under pressure. Proceedings of the National Academy of Sciences, 119, e2117416119, https://doi.org/10.1073/pnas.2117416119.
Dorogova, M., Navrotsky, A., and Boatner, L.A. (2007) Enthalpies of formation of rare earth orthovanadates, $REVO_4$. Journal of Solid State Chemistry, 180, 847–851, https://doi.org/10.1016/j.jssc.2006.12.001.
Du, J., Devanathan, R., René Corrales, L., and Weber, W.J. (2012) First-principles calculations of the electronic structure, phase transition and properties of $ZrSiO_4$ polymorphs. Computational & Theoretical Chemistry, 987, 62–70, https://doi.org/10.1016/j.comptc.2011.03.033.
Ehlers, A.M., Zaffiro, G., Angel, R.J., Boffa-Ballaran, T., Carpenter, M.A., Alvaro, M., and Ross, N.L. (2022) Thermoelastic properties of zircon: Implications for geothermobarometry. American Mineralogist, 107, 74–81, https://doi.org/10.2138/

am-2021-7731.
Ellison, A.J.G. and Navrotsky, A. (1992) Enthalpy of formation of zircon. Journal of the American Ceramic Society, 75, 1430–1433, https://doi.org/10.1111/j.1151-2916.1992.tb04205.x.
Ellsworth, S., Navrotsky, A., and Ewing, R.C. (1994) Energetics of radiation damage in natural zircon ($ZrSiO_4$). Physics and Chemistry of Minerals, 21, 140–149, https://doi.org/10.1007/BF00203144.
Ennaciri, A., Kahn, A., and Michel, D. (1986) Crystal structures of $HfGeO_4$ and $ThGeO_4$ germanates. Journal of the Less Common Metals, 124, 105–109, https://doi.org/10.1016/0022-5088(86)90481-9.
Errandonea, D. (2015) Exploring the properties of MTO_4 compounds using high-pressure powder X-ray diffraction. Crystal Research and Technology, 50, 729–736, https://doi.org/10.1002/crat.201500010.
——— (2017) High-pressure phase transitions and properties of MTO_4 compounds with the monazite-type structure. Physica status solidi (b), 254, 1700016, https://doi.org/10.1002/pssb.201700016.
Errandonea, D. and Garg, A.B. (2018) Recent progress on the characterization of the high-pressure behaviour of AVO_4 orthovanadates. Progress in Materials Science, 97, 123–169, https://doi.org/10.1016/j.pmatsci.2018.04.004.
Errandonea, D. and Manjón, F.J. (2008) Pressure effects on the structural and electronic properties of ABX_4 scintillating crystals. Progress in Materials Science, 53, 711–773, https://doi.org/10.1016/j.pmatsci.2008.02.001.
Errandonea, D., Kumar, R.S., Gracia, L., Beltrán, A., Achary, S.N., and Tyagi, A.K. (2009a) Experimental and theoretical investigation of $ThGeO_4$ at high pressure. Physical Review B: Condensed Matter and Materials Physics, 80, 1–7, https://doi.org/10.1103/PhysRevB.80.094101.
Errandonea, D., Lacomba-Perales, R., Ruiz-Fuertes, J., Segura, A., Achary, S.N., and Tyagi, A.K. (2009b) High-pressure structural investigation of several zircon-type orthovanadates. Physical Review B: Condensed Matter and Materials Physics, 79, 1–9, https://doi.org/10.1103/PhysRevB.79.184104.
Errandonea, D., Kumar, R.S., Achary, S.N., and Tyagi, A.K. (2011) In situ high-pressure synchrotron X-ray diffraction study of $CeVO_4$ and $TbVO_4$ up to 50 GPa. Physical Review B: Condensed Matter and Materials Physics, 84, 1–8, https://doi.org/10.1103/PhysRevB.84.224121.
Errandonea, D., Popescu, C., Achary, S.N., Tyagi, A.K., and Bettinelli, M. (2014) In situ high-pressure synchrotron X-ray diffraction study of the structural stability in $NdVO_4$ and $LaVO_4$. Materials Research Bulletin, 50, 279–284, https://doi.org/10.1016/j.materresbull.2013.10.047.
Estevenon, P., Welcomme, E., Szenknect, S., Mesbah, A., Moisy, P., Poinssot, C., and Dacheux, N. (2018) Multiparametric study of the synthesis of $ThSiO_4$ under hydrothermal conditions. Inorganic Chemistry, 57, 9393–9402, https://doi.org/10.1021/acs.inorgchem.8b01390.
——— (2019a) Preparation of $CeSiO_4$ from aqueous precursors under soft hydrothermal conditions. Dalton Transactions, 48, 7551–7559, https://doi.org/10.1039/C9DT01258C.
Estevenon, P., Kaczmarek, T., Vadot, F., Dumas, T., Solari, P.L., Welcomme, E., Szenknect, S., Mesbah, A., Moisy, P., Poinssot, C., and others. (2019b) Formation of $CeSiO_4$ from cerium(III) silicate precursors. Dalton Transactions, 48, 10455–10463, https://doi.org/10.1039/C9DT01990A.
Estevenon, P., Kaczmarek, T., Rafiuddin, M.R., Welcomme, E., Szenknect, S., Mesbah, A., Moisy, P., Poinssot, C., and Dacheux, N. (2020a) Soft hydrothermal synthesis of hafnon, $HfSiO_4$. Crystal Growth & Design, 20, 1820–1828, https://doi.org/10.1021/acs.cgd.9b01546.
Estevenon, P., Welcomme, E., Tamain, C., Jouan, G., Szenknect, S., Mesbah, A., Poinssot, C., Moisy, P., and Dacheux, N. (2020b) The formation of $PuSiO_4$ under hydrothermal conditions. Dalton Transactions, 49, 6434–6445, https://doi.org/10.1039/D0DT01183E.
Estevenon, P., Dumas, T., Solari, P.L., Welcomme, E., Szenknect, S., Mesbah, A., Kvashnina, K.O., Moisy, P., Poinssot, C., and Dacheux, N. (2021a) Formation of plutonium(IV) silicate species in very alkaline reactive media. Dalton Transactions, 50, 12528–12536, https://doi.org/10.1039/D1DT02248B.
——— (2021b) Correction: Formation of plutonium(iv) silicate species in very alkaline reactive media. Dalton Transactions, 50, 12528–12536, https://doi.org/10.1039/D1DT02248B.
Ewing, R.C. (1999) Nuclear waste forms for actinides. Proceedings of the National Academy of Sciences, 96, 3432–3439, https://doi.org/10.1073/pnas.96.7.3432.
——— (2015) Long-term storage of spent nuclear fuel. Nature Materials, 14, 252–257, https://doi.org/10.1038/nmat4226.
——— (2007) Displaced by radiation. Nature, 445, 161–162, https://doi.org/10.1038/445161a.
Ewing, R.C., Haaker, R.F., and Lutze, W. (1982) Leachability of zircon as a function of alpha dose. In W. Lutze, Ed., Scientific Basis for Radioactive Waste Management, 389–397. Elsevier.
Ewing, R.C., Weber, W.J., and Clinard, F.W. Jr. (1995a) Radiation effects in nuclear waste forms for high-level radioactive waste. Progress in Nuclear Energy, 29, 63–127, https://doi.org/10.1016/0149-1970(94)00016-Y.
Ewing, R.C., Lutze, W., and Weber, W.J. (1995b) Zircon: A host-phase for the disposal of weapons plutonium. Journal of Materials Research, 10, 243–246, https://doi.org/10.1557/JMR.1995.0243.
Ewing, R.C., Meldrum, A., Wang, L.M., Weber, W.J., and Corrales, L.R. (2003) Radiation effects in zircon In J.M. Hanchar and P.W.O. Hoskin, Eds., Zircon, 53, 387–425. Reviews in Mineralogy and Geochemistry, Mineralogical Society of America, Chantilly, Virginia.
Farnan, I., Balan, E., Pickard, C.J., and Mauri, F. (2003) The effect of radiation on local structure in the crystalline fraction of $ZrSiO_4$: Investigating the ^{29}Si NMR response to pressure in zircon and reidite. American Mineralogist, 88, 1663–1667, https://doi.org/10.2138/am-2003-11-1205.
Ferriss, E.D.A., Ewing, R.C., and Becker, U. (2010) Simulation of thermodynamic mixing properties of actinide-containing zircon solid solutions. American Mineralogist, 95, 229–241, https://doi.org/10.2138/am.2010.3318.
Finch, R.J. and Hanchar, J.M. (2003) Structure and chemistry of zircon and zircon-group minerals. In J.M. Hanchar and P.W.O. Hoskin, Eds., Zircon, 53, 1–26. Reviews in Mineralogy and Geochemistry, Mineralogical Society of America, Chantilly, Virginia.
Finch, C.B., Harris, L.A., and Clark, G.W. (1964) The thorite → huttonite phase transformation as determined by growth of synthetic thorite and huttonite single crystals. American Mineralogist, 49, 782–785.
Fuchs, L.H. and Gebert, E. (1958) X-ray studies of synthetic coffinite, thorite, and uranothorites. American Mineralogist, 43, 243–248.
Fuchs, L.H. and Hoekstra, H.R. (1959) The preparation and properties of uranium (IV) silicate. American Mineralogist, 44, 1057–1063.
Fuhrmann, J. and Pickardt, J. (1986) Bildung von $HfSiO_4$-einkristallen durch chemische transportreaktion. ZAAC—Zeitschrift für Anorganische und Allgemeine Chemie, 532, 171–174, https://doi.org/10.1002/zaac.19865320123.
Garg, A.B. and Errandonea, D. (2015) High-pressure powder X-ray diffraction study of $EuVO_4$. Journal of Solid State Chemistry, 226, 147–153, https://doi.org/10.1016/j.jssc.2015.02.003.
Garg, A.B., Rao, R., Sakuntala, T., Wani, B.N., and Vijayakumar, V. (2009) Phase stability of $YbVO_4$ under pressure: In situ X-ray and Raman spectroscopic investigations. Journal of Applied Physics, 106, 063513, https://doi.org/10.1063/1.3223327.
Garg, A.B., Shanavas, K.V., Wani, B.N., and Sharma, S.M. (2013) Phase transition and possible metallization in $CeVO_4$ under pressure. Journal of Solid State Chemistry, 203, 273–280, https://doi.org/10.1016/j.jssc.2013.04.036.
Garg, A.B., Errandonea, D., Rodríguez-Hernández, P., López-Moreno, S., Muñoz, A., and Popescu, C. (2014) High-pressure structural behaviour of $HoVO_4$: Combined XRD experiments and ab initio calculations. Journal of Physics: Condensed Matter, 26, 265402, https://doi.org/10.1088/0953-8984/26/26/265402.
Gavrichev, K.S., Smirnova, N.N., Gurevich, V.M., Danilov, V.P., Tyurin, A.V., Ryumin, M.A., and Komissarova, L.N. (2006) Heat capacity and thermodynamic functions of $LuPO_4$ in the range 0–320 K. Thermochimica Acta, 448, 63–65, https://doi.org/10.1016/j.tca.2006.05.019.
Gavrichev, K.S., Ryumin, M.A., Tyurin, A.V., Gurevich, V.M., and Komissarova, L.N. (2010a) Heat capacity and thermodynamic functions of pretulite $ScPO_4$(c) at 0–1600 K. Geochemistry International, 48, 390–397, https://doi.org/10.1134/S0016702910040075.
——— (2010b) Heat capacity and thermodynamic functions of xenotime YPO_4(c) at 0–1600 K. Geochemistry International, 48, 932–939, https://doi.org/10.1134/S0016702910090065.
——— (2010c) Heat capacity and thermodynamic functions of YVO_4 in the 13–347 K region. Russian Journal of Inorganic Chemistry, 55, 1935–1939, https://doi.org/10.1134/S0036023610120181.
——— (2011) Revised heat capacity and thermodynamic functions of $GdVO_4$. Inorganic Materials, 47, 1120–1125, https://doi.org/10.1134/S0020168511090081.
Gavrichev, K.S., Ryumin, M.A., Tyurin, A.V., Gurevich, V.M., Khoroshilov, A.V., and Komissarova, L.N. (2012a) Thermodynamic functions of erbium orthophosphate $ErPO_4$ in the temperature range of 0–1600 K. Thermochimica Acta, 535, 1–7, https://doi.org/10.1016/j.tca.2012.02.002.
Gavrichev, K.S., Ryumin, M.A., Tyurin, A.V., Gurevich, V.M., Solov'ev, O.I., and Komissarova, L.N. (2012b) Thermodynamic functions of $ScVO_4$ at temperatures from 0 to 350 K. Inorganic Materials, 48, 845–850, https://doi.org/10.1134/S0020168512070059.
Gavrichev, K.S., Ryumin, M.A., Tyurin, A.V., Gurevich, V.M., Nikiforova, G.E., and Komissarova, L.N. (2013a) Heat capacity and thermodynamic functions of $YbPO_4$ from 0 to 1800 K. Inorganic Materials, 49, 701–708, https://doi.org/10.1134/S0020168513070042.
——— (2013b) Heat capacity and thermodynamic functions of $YbPO_4$ from 0 to 1800 K. Inorganic Materials, 49, 701–708, https://doi.org/10.1134/S0020168513070042.
Gavrichev, K.S., Ryumin, M.A., Gurevich, V.M., and Tyurin, A.V. (2014) Low-temperature heat capacity and thermodynamic functions of $DyVO_4$. Inorganic Materials, 50, 917–923, https://doi.org/10.1134/S0020168514090039.
Geisler, T., Burakov, B., Yagovkina, M., Garbuzov, V., Zamoryanskaya, M., Zirlin, V., and Nikolaeva, L. (2005) Structural recovery of self-irradiated natural and ^{238}Pu-doped zircon in an acidic solution at 175°C. Journal of Nuclear Materials, 336, 22–30, https://doi.org/10.1016/j.jnucmat.2004.08.005.
Geisler, T., Schaltegger, U., and Tomaschek, F. (2007) Re-equilibration of zircon in aqueous fluids and melts. Elements, 3, 43–50, https://doi.org/10.2113/gselements.3.1.43.
Glass, B.P., Liu, S., and Leavens, P.B. (2002) Reidite: An impact-produced high-pressure polymorph of zircon found in marine sediments. American Mineralogist, 87, 562–565, https://doi.org/10.2138/am-2002-0420.
Glasser, L. (2011) Thermodynamics of condensed phases: Formula unit volume, V_m, and

the determination of the number of formula units, *Z*, in a crystallographic unit cell. Journal of Chemical Education, 88, 581–585, https://doi.org/10.1021/ed900046k.

Gleissner, J., Errandonea, D., Segura, A., Pellicer-Porres, J., Hakeem, M.A., Proctor, J.E., Raju, S.V., Kumar, R.S., Rodríguez-Hernández, P., Muñoz, A., and others. (2016) Monazite-type $SrCrO_4$ under compression. Physical Review B: Condensed Matter and Materials Physics, 94, 134108, https://doi.org/10.1103/PhysRevB.94.134108.

Goel, A., McCloy, J.S., Pokorny, R., and Kruger, A.A. (2019) Challenges with vitrification of Hanford High-Level Waste (HLW) to borosilicate glass—An overview. Journal of Non-Crystalline Solids: X, 4, 1–19.

Golbs, S., Cardoso-Gil, R., and Schmidt, M. (2009) Crystal structure of europium arsenate, $EuAsO_4$. Zeitschrift für Kristallographie, 224, 169–170, https://doi.org/10.1524/ncrs.2009.0076.

Goldwin, B.A., Yushkin, N.P., and Fishman, M.V. (1976) A new ytrrium mineral, chernovite. Zapiski Vserossiskogo Mineralogicheskogo Obshchetstva, 699–704.

Gomis, O., Lavina, B., Rodríguez-Hernández, P., Muñoz, A., Errandonea, R., Errandonea, D., and Bettinelli, M. (2017) High-pressure structural, elastic, and thermodynamic properties of zircon-type $HoPO_4$ and $TmPO_4$. Journal of Physics: Condensed Matter, 29, 095401, https://doi.org/10.1088/1361-648X/aa516a.

Goncharov, V.G., Wei, N., Lau, M.L., Ennaceur, S.M., Migliori, A., Xu, H., Long, M., and Guo, X. (2021) Elastic and thermodynamic properties of cerium-doped yttrium aluminum garnets. Journal of the American Ceramic Society, 104, 3478–3496, https://doi.org/10.1111/jace.17679.

Goncharov, V.G., Nisbet, H.D., Strzelecki, A.C., Benmore, C.J., Migdisov, A., Xu, H., and Guo, X. (2022) Energetics of hydroxylbastnäsite solid solutions, $La_{1-x}Nd_xCO_3OH$. Geochimica et Cosmochimica Acta, 330, 47–66, https://doi.org/10.1016/j.gca.2022.04.002.

Graeser, S., Schwander, H., and Stalder, H.A. (1973) A solid solution series between xenotime ($YtPO_4$) and chernovite ($YtAsO_4$). Mineralogical Magazine, 39, 145–151, https://doi.org/10.1180/minmag.1973.039.302.02.

Grenthe, I., Fuger, J., Konings, R.J.M., Lemire, R.J., Muller, A.B., Nguyen-Trung, C., and Wanner, H. (1993) Chemical Thermodynamics of Uranium, p. 715. North-Holland.

Grover, V. and Tyagi, A.K. (2005) Preparation and bulk thermal expansion studies in $M_{1-x}Ce_xSiO_4$ (M = Th, Zr) system, and stabilization of tetragonal $ThSiO_4$. Journal of Alloys and Compounds, 390, 112–114, https://doi.org/10.1016/j.jallcom.2004.05.091.

Gucsik, A., Zhang, M., Koeberl, C., Salje, E.K.H., Redfern, S.A.T., and Pruneda, J.M. (2004) Infrared and Raman spectra of $ZrSiO_4$ experimentally shocked at high pressures. Mineralogical Magazine, 68, 801–811, https://doi.org/10.1180/0026461046850220.

Guedes, I., Hirano, Y., Grimsditch, M., Wakabayashi, N., Loong, C.K., and Boatner, L.A. (2001) Raman study of phonon modes in $ErVO_4$ single crystals. Journal of Applied Physics, 90, 1843–1846, https://doi.org/10.1063/1.1384858.

Guo, X. and Xu, H. (2017) Enthalpies of formation of polyhalite: A mineral relevant to salt repository. The Journal of Chemical Thermodynamics, 114, 44–47, https://doi.org/10.1016/j.jct.2017.05.031.

Guo, X., Tavakoli, A.H., Sutton, S., Kukkadapu, R.K., Qi, L., Lanzirotti, A., Newville, M., Asta, M., and Navrotsky, A. (2014) Cerium substitution in yttrium iron garnet: Valence state, structure, and energetics. Chemistry of Materials, 26, 1133–1143, https://doi.org/10.1021/cm403444f.

Guo, X., Szenknect, S., Mesbah, A., Labs, S., Clavier, N., Poinssot, C., Ushakov, S.V., Curtius, H., Bosbach, D., Ewing, R.C., and others. (2015) Thermodynamics of formation of coffinite, $USiO_4$. Proceedings of the National Academy of Sciences, 112, 6551–6555, https://doi.org/10.1073/pnas.1507441112.

Guo, X., Szenknect, P., Mesbah, A., Clavier, N., Poinssot, C., Wu, D., Xu, H., Dacheux, N., Ewing, R.C., and Navrotsky, A. (2016a) Energetics of a uranothorite ($Th_{1-x}U_xSiO_4$) solid solution. Chemistry of Materials, 28, 7117–7124, https://doi.org/10.1021/acs.chemmater.6b03346.

Guo, X., Tiferet, E., Qi, L., Solomon, J.M., Lanzirotti, A., Newville, M., Engelhard, M.H., Kukkadapu, R.K., Wu, D., Ilton, E.S., and others. (2016b) U(v) in metal uranates: A combined experimental and theoretical study of $MgUO_4$, $CrUO_4$, and $FeUO_4$. Dalton Transactions, 45, 4622–4632, https://doi.org/10.1039/C6DT00066E.

Gysi, A.P. and Harlov, D. (2021) Hydrothermal solubility of $TbPO_4$, $HoPO_4$, $TmPO_4$, and $LuPO_4$ xenotime endmembers at pH of 2 and temperatures between 100 and 250 °C. Chemical Geology, 567, 120072, https://doi.org/10.1016/j.chemgeo.2021.120072.

Gysi, A.P., Williams-Jones, A.E., and Harlov, D. (2015) The solubility of xenotime-(Y) and other HREE phosphates ($DyPO_4$, $ErPO_4$ and $YbPO_4$) in aqueous solutions from 100 to 250 °C and p_{sat}. Chemical Geology, 401, 83–95, https://doi.org/10.1016/j.chemgeo.2015.02.023.

Gysi, A.P., Harlov, D., Filho, D.C., and Williams-Jones, A.E. (2016) Experimental determination of the high temperature heat capacity of a natural xenotime-(Y) solid solution and synthetic $DyPO_4$ and $ErPO_4$ endmembers. Thermochimica Acta, 627–629, 61–67, https://doi.org/10.1016/j.tca.2016.01.016.

Gysi, A.P., Van Hoozen, C., and Harlov, D. (2021) Hydrothermal solubility of $TbPO_4$, $HoPO_4$, $TmPO_4$, and $LuPO_4$ xenotime endmembers at pH of 2 and temperatures between 100 and 250 °C. Chemical Geology, 567, 120072.

Hanchar, J.M. and Watson, E.B. (2003) Zircon saturation thermometry. In J.M. Hanchar and P.W.O. Hoskin, Eds., Zircon, 53, 89–112. Reviews in Mineralogy and Geochemistry, Mineralogical Society of America, Chantilly, Virginia.

Hanchar, J.M., Burakov, B.E., Anderson, E.B., and Zamoryanskaya, M.V. (2003) Investigation of single crystal zircon, $(Zr,Pu)SiO_4$, Doped with ^{238}Pu. Materials Research Society Symposium Proceedings, 757, 1–11.

Hansley, P.L. and Fitzpatrick, J.J. (1989) Compositional and crystallographic data on REE-bearing coffinite from the Grants uranium region, northwestern New Mexico. American Mineralogist, 74, 263–270.

Harley, S.L. and Kelly, N.M. (2007) Zircon tiny but timely. Elements, 3, 13–18, https://doi.org/10.2113/gselements.3.1.13.

Harlov, D.E., Wirth, R., and Hetherington, C.J. (2007) The relative stability of monazite and huttonite at 300–900 °C and 200–1000 MPa: Metasomatism and the propagation of metastable mineral phases. American Mineralogist, 92, 1652–1664, https://doi.org/10.2138/am.2007.2459.

Hazen, R.M. (1977) Temperature, pressure, and composition: Structurally analogous variables. Physics and Chemistry of Minerals, 1, 83–94, https://doi.org/10.1007/BF00307981.

Hazen, R.M. and Finger, L.M. (1979) Crystal structure and compressibility of zircon at high pressure. American Mineralogist, 64, 196–201.

Helean, K.B. and Navrotsky, A. (2002) Oxide melt solution calorimetry of rare earth oxides. Journal of Thermal Analysis and Calorimetry, 69, 751–771, https://doi.org/10.1023/A:1020687418374.

Helean, K.B., Navrotsky, A., Lumpkin, G.R., Colella, M., Lian, J., Ewing, R.C., Ebbinghaus, B., and Catalano, J.G. (2003) Enthalpies of formation of U-, Th-, Ce-brannerite: Implications for plutonium immobilization. Journal of Nuclear Materials, 320, 231–244, https://doi.org/10.1016/S0022-3115(03)00186-7.

Helean, K.B., Ushakov, S.V., Brown, C.E., Navrotsky, A., Lian, J., Ewing, R.C., Farmer, J.M., and Boatner, L.A. (2004) Formation enthalpies of rare earth titanate pyrochlores. Journal of Solid State Chemistry, 177, 1858–1866, https://doi.org/10.1016/j.jssc.2004.01.009.

Heuser, J.M., Palomares, R.I., Bauer, J.D., Rodriguez, M.J.L., Cooper, J., Lang, M., Scheinost, A.C., Schlenz, H., Winkler, B., Bosbach, D., and others. (2018) Structural characterization of $(Sm,Tb)PO_4$ solid solutions and pressure-induced phase transitions. Journal of the European Ceramic Society, 38, 4070–4081, https://doi.org/10.1016/j.jeurceramsoc.2018.04.030.

Hikichi, Y. and Nomura, T. (1987) Melting temperatures of monazite and xenotime. Journal of the American Ceramic Society, 70, C-252–C-253, https://doi.org/10.1111/j.1151-2916.1987.tb04890.x.

Hirano, Y., Guedes, I., Grimsditch, M., Loong, C.-K., Wakabayashi, N., and Boatner, L.A. (2002a) Brillouin-scattering study of the elastic constants of $ErVO_4$. Journal of the American Ceramic Society, 85, 1001–1003, https://doi.org/10.1111/j.1151-2916.2002.tb00209.x.

Hirano, Y., Skanthakumar, S., Loong, C.K., Wakabayashi, N., and Boatner, L.A. (2002b) Lattice and magnetic properties of $ErVO_4$ and $ErPO_4$. Physical Review B: Condensed Matter and Materials Physics, 66, 244241–244247, https://doi.org/10.1103/PhysRevB.66.024424.

Hoekstra, H.R. and Fuchs, L.H. (1956) Synthesis of coffinite—$USiO_4$. Science, 123, 105, https://doi.org/10.1126/science.123.3186.105.a.

Hoskin, P.W.O. and Schaltegger, U. (2003) The composition of zircon and igneous and metamorphic petrogenesis. In J.M. Hanchar and P.W.O. Hoskin, Eds., Zircon, 53, 27–62. Reviews in Mineralogy and Geochemistry, Mineralogical Society of America, Chantilly, Virginia.

Huang, Z., Zhang, L., Feng, J., Cui, X., and Pan, W. (2012a) Electronic, elastic and optical properties of zircon $GdVO_4$ investigated from experiments and LSDA+U. Journal of Alloys and Compounds, 538, 56–60, https://doi.org/10.1016/j.jallcom.2012.05.103.

Huang, Z., Zhang, L., and Pan, W. (2012b) Synthesis, lattice dynamics, and mechanical properties of a high-pressure scheelite phase of RVO_4. Inorganic Chemistry, 51, 11235–11237, https://doi.org/10.1021/ic3017672.

Ireland, T.R. and Williams, I.S. (2003) Considerations in zircon geochronology by SIMS. In J.M. Hanchar and P.W.O. Hoskin, Eds., Zircon, 53, 215–242. Reviews in Mineralogy and Geochemistry, Mineralogical Society of America, Chantilly, Virginia.

Janeczek, J. (1991) Composition and origin of coffinite from Jachymov, Czechoslovakia. Neues Jahrbuch für Mineralogie Monatshefte, 9, 385–395.

Jellison, G.E. Jr., Boatner, L.A., and Chen, C. (2000) Spectroscopic refractive indices of metalorthophosphates with the zircon-type structure. Optical Materials, 15, 103–109, https://doi.org/10.1016/S0925-3467(00)00027-6.

Jenkins, H.D.B. and Glasser, L. (2003) Standard absolute entropy, S°_{298}, values from volume or density. Inorganic Chemistry, 42, 8702–8708, https://doi.org/10.1021/ic030219p.

Ji, Y., Kowalski, P.M., Kegler, P., Huittinen, N., Marks, N.A., Vinograd, V.L., Arinicheva, Y., Neumeier, S., and Bosbach, D. (2019) Rare-earth orthophosphates from atomistic simulations. Frontiers in Chemistry, 7, 197, https://doi.org/10.3389/fchem.2019.00197.

Jiménez, E., Isasi, J., and Sáez-Puche, R. (2000) Synthesis, structural characterization and magnetic properties of $RCrO_4$ oxides, R = Nd, Sm, Eu and Lu. Journal of Alloys and Compounds, 312, 53–59, https://doi.org/10.1016/S0925-8388(00)01079-3.

——— (2002) Field-induced magnetic properties in $RCrO_4$ oxides (R = Pr, Gd, Tb, Tm, and Yb). Journal of Solid State Chemistry, 164, 313–319.

Kang, D.H. and Schleid, T. (2005) Einkristalle von $La[AsO_4]$ im monazit- und $Sm[AsO_4]$ im xenotim-typ. Zeitschrift für Anorganische und Allgemeine Chemie, 631, 1799–1802, https://doi.org/10.1002/zaac.200500209.

Kang, D.-H., Hoss, P., and Schleid, T. (2005) Xenotime-type $Yb[AsO_4]$ Dong-Hee. Acta Crystallographica Section E, 61, i270–i272, https://doi.org/10.1107/S1600536805036457.

Keller, V.C. (1963) Untersuchungen über die Germanate und Silikate des typs ABO_4 der vierwertigen Elemente Thorium bis Americium. Nukleonik, 41–48.

Kijkowska, R. (2003) Thermal decomposition of lanthanide orthophosphates synthesized through crystallization from phosphoric acid solution. Thermochimica Acta, 404, 81–88, https://doi.org/10.1016/S0040-6031(03)00085-6.

Knittle, E. and Williams, Q. (1993) High-pressure Raman spectroscopy of $ZrSiO_4$: Observation of the zircon to scheelite transition at 300 K. American Mineralogist, 78, 245–252.

Knyazev, A.V., Komshina, M.E., and Savushkin, I.A. (2017) Synthesis and high-temperature X-ray diffraction study of thorium orthosilicate. Radiochemistry, 59, 225–228, https://doi.org/10.1134/S106636221703002X.

Kogawa, M., Watson, E.B., Ewing, R.C., and Utsunomiya, S. (2012) Lead in zircon at the atomic scale. American Mineralogist, 97, 1094–1102, https://doi.org/10.2138/am.2012.3993.

Kohn, M.J., Engi, M., and Lanari, P., Eds. (2017) Petrochronology, 596 p. De Gruyter.

Kolitsch, U. and Holtstam, D. (2004) Crystal chemistry of $REEXO_4$ compounds (X = P,As,V). II. Review of $REEXO_4$ compounds and their stability fields. European Journal of Mineralogy, 16, 117–126, https://doi.org/10.1127/0935-1221/2004/0016-0117.

Konings, R. and Plyasunov, A. (2017) Comment on "First experimental determination of the solubility constant of coffinite" [Geochim. Cosmochim. Acta 181 (2016) 36–53]. Geochimica et Cosmochimica Acta, 212, 372–373, https://doi.org/10.1016/j.gca.2017.03.018.

Konings, R.J.M., Beneš, O., Kovács, A., Manara, D., Sedmidubský, D., Gorokhov, L., Iorish, V.S., Yungman, V., Shenyavskaya, E., and Osina, E. (2014) The thermodynamic properties of the *f*-Elements and their Compounds: Part 2. The Lanthanide and Actinide Oxides. Journal of Physical and Chemical Reference Data, 43, 013101, https://doi.org/10.1063/1.4825256.

Konno, H., Aoki, Y., Klencsár, Z., Vértes, A., Wakeshima, M., Tezuka, K., and Hinatsu, Y. (2001) Structure of $EuCrO_4$ and its electronic and magnetic properties. Bulletin of the Chemical Society of Japan, 74, 2335–2341, https://doi.org/10.1246/bcsj.74.2335.

Kramers, J., Frei, R., Newville, M., Kober, B., and Villa, I. (2009) On the valency state of radiogenic lead in zircon and its consequences. Chemical Geology, 261, 4–11, https://doi.org/10.1016/j.chemgeo.2008.09.010.

Kusaba, K., Syono, Y., Kikuchi, M., and Fukuoka, K. (1985) Shock behavior of zircon: Phase transition to scheelite structure and decomposition. Earth and Planetary Science Letters, 72, 433–439, https://doi.org/10.1016/0012-821X(85)90064-0.

Labs, S., Hennig, C., Weiss, S., Curtius, H., Zänker, H., and Bosbach, D. (2014) Synthesis of coffinite, $USiO_4$, and structural investigations of $U_xTh_{(1-x)}SiO_4$ solid solutions. Environmental Science & Technology, 48, 854–860, https://doi.org/10.1021/es403995b.

Lacomba-Perales, R., Errandonea, D., Meng, Y., and Bettinelli, M. (2010) High-pressure stability and compressibility of APO_4 (A=La, Nd, Eu, Gd, Er, and Y) orthophosphates: An X-ray diffraction study using synchrotron radiation. Physical Review B: Condensed Matter and Materials Physics, 81, 064113, https://doi.org/10.1103/PhysRevB.81.064113.

Langmuir, D. (1978) Uranium solution-mineral equilibria at low temperatures with applications to sedimentary ore deposits. Geochimica et Cosmochimica Acta, 42, 547–569, https://doi.org/10.1016/0016-7037(78)90001-7.

Langmuir, D. and Chatham, J.R. (1980) Groundwater prospecting for sandstone-type uranium deposits: A preliminary comparison of the merits of mineral-solution equilibria, and single-element tracer methods. Journal of Geochemical Exploration, 13, 201–219, https://doi.org/10.1016/0375-6742(80)90007-2.

Ledderboge, F., Nowak, J., Massonne, H.J., Förg, K., Höppe, H.A., and Schleid, T. (2018) High-pressure investigations of yttrium(III) oxoarsenate(V): Crystal structure and luminescence properties of Eu^{3+}-doped scheelite-type $Y[AsO_4]$ from xenotime-type precursors. Journal of Solid State Chemistry, 263, 65–71, https://doi.org/10.1016/j.jssc.2018.03.002.

Lee, Y.M. and Nassaralla, C.L. (2006) Standard free energy of formation of calcium chromate. Materials Science and Engineering A, 437, 334–339, https://doi.org/10.1016/j.msea.2006.08.010.

Leeman, W.P. and Sisson, V.B. (1996) Geochemistry of boron and its implications for crustal and mantle processes. Reviews in Mineralogy, 33, 644–707.

Lentz, A., Buchele, W., and Schollhorn, H. (1986) Crystal growth from silica gels and single crystal structure of bariumchromate. Crystal Research and Technology, 21, 827–833, https://doi.org/10.1002/crat.2170210704.

Li, L., Yu, W., Long, Y., and Jin, C. (2006) First-principles calculations on the pressure induced zircon-type to scheelite-type phase transition of $CaCrO_4$. Solid State Communications, 137, 358–361, https://doi.org/10.1016/j.ssc.2005.12.021.

Li, H., Zhou, S., and Zhang, S. (2007) The relationship between the thermal expansions and structures of ABO_4 oxides. Journal of Solid State Chemistry, 180, 589–595, https://doi.org/10.1016/j.jssc.2006.11.023.

Li, H., Zhang, S., Zhou, S., and Cao, X. (2009) Bonding characteristics, thermal expansibility, and compressibility of $RXO_{(4)}$ (R = rare earths, X = P, As) within monazite and zircon structures. Inorganic Chemistry, 48, 4542–4548, https://doi.org/10.1021/ic900337j.

Li, K., Ding, Z., and Xue, D. (2011) Electronegativity-related bulk moduli of crystal materials. Physica status solidi (b), Basin Research, 248, 1227–1236.

Li, H., Noh, H.M., Moon, B.K., Choi, B.C., and Jeong, J.H. (2014) Chemical bonding characterization, expansivity and compressibility of $RECrO_4$. Journal of Alloys and Compounds, 582, 151–156, https://doi.org/10.1016/j.jallcom.2013.08.006.

Lohmüller, G., Schmidt, G., Deppisch, B., Gramlich, V., and Scheringer, C. (1973) Die kristallstrukturen von yttrium-vanadat, lutetium-phosphat und lutetium-arsenat. Acta Crystallographica Section B, 29, 141–142, https://doi.org/10.1107/S0567740873002098.

Long, F.G. and Stager, C.V. (1977) Low temperature crystal structure of $TbAsO_4$ and $DyAsO_4$. Canadian Journal of Physics, 55, 1633–1640.

Long, Y.W., Yang, L.X., You, S.J., Yu, Y., Yu, R.C., Jin, C.Q., and Liu, J. (2006) Crystal structural phase transition in $CaCrO_4$ under high pressure. Journal of Physics: Condensed Matter, 18, 2421–2428, https://doi.org/10.1088/0953-8984/18/8/008.

Long, Y.W., Yang, L.X., Yu, Y., Li, F.Y., Yu, R.C., and Jin, C.Q. (2007) Synthesis, structure, magnetism and specific heat of $YCrO_4$ and its zircon-to-scheelite phase transition. Physical Review B: Condensed Matter and Materials Physics, 75, 104402, https://doi.org/10.1103/PhysRevB.75.104402.

Loong, C.K., Soderholm, L., Hammonds, J.P., Abraham, M.M., Boatner, L.A., and Edelstein, N.M. (1993) Rare-earth energy levels and magnetic properties of $HoPO_4$ and $ErPO_4$. Journal of Physics: Condensed Matter, 5, 5121–5140, https://doi.org/10.1088/0953-8984/5/29/009.

López-Solano, J., Rodríguez-Hernández, P., Muñoz, A., Gomis, O., Santamaría-Perez, D., Errandonea, D., Manjón, F.J., Kumar, R.S., Stavrou, E., and Raptis, C. (2010) Theoretical and experimental study of the structural stability of $TbPO_4$ at high pressures. Physical Review B: Condensed Matter and Materials Physics, 81, 144126, https://doi.org/10.1103/PhysRevB.81.144126.

Lü, X., Stoumpos, C., Hu, Q., Ma, X., Zhang, D., Guo, S., Hoffman, J., Bu, K., Guo, X., Wang, Y., and others. (2021) Regulating off-centering distortion maximizes photoluminescence in halide perovskites. National Science Review, 8, nwaa288.

Luo, W. and Ahuja, R. (2008) High pressure structural phase transition in zircon ($ZrSiO_4$). Journal of Physics: Conference Series, 121, 0220014, https://doi.org/10.1088/1742-6596/121/2/022014.

Manjón, F.J., Errandonea, D., Garro, N., Pellicer-Porres, J., Rodríguez-Hernández, P., Radescu, S., López-Solano, J., Mujica, A., and Muñoz, A. (2006a) Lattice dynamics study of scheelite tungstates under high pressure I. $BaWO_4$. Physical Review B: Condensed Matter and Materials Physics, 74, 144111.

Manjón, F.J., Errandonea, D., Garro, N., Pellicer-Porres, J., López-Solano, J., Rodríguez-Hernández, P., Radescu, S., Mujica, A., and Muñoz, A. (2006b) Lattice dynamics study of scheelite tungstates under high pressure II. $PbWO_4$. Physical Review B: Condensed Matter and Materials Physics, 74, 144112.

Manoun, B., Downs, R.T., and Saxena, S.K. (2006) A high-pressure Raman spectroscopic study of hafnon, $HfSiO_4$. American Mineralogist, 91, 1888–1892, https://doi.org/10.2138/am.2006.2070.

Marcial, J., Zhang, Y., Zhao, X., Xu, H., Mesbah, A., Nienhuis, E.T., Szenknect, S., Neuefeind, J.C., Lin, J., Qi, L., and others. (2021) Thermodynamic nonideality and disorder heterogeneity in actinide silicate solid solutions. Materials Degradation, 5, 34.

Marinova, L.A., Glibin, V.P., and Volkov, A.I. (1973) No Title. Rassh. Tezisi. Dokl. Tbilissi Meznierba.

Mazeina, L., Ushakov, S.V., Navrotsky, A., and Boatner, L.A. (2005) Formation enthalpy of $ThSiO_4$ and enthalpy of the thorite → huttonite phase transition. Geochimica et Cosmochimica Acta, 69, 4675–4683, https://doi.org/10.1016/j.gca.2005.03.053.

McMurdie, H.F. and Hall, F.P. (1947) Phase diagrams for ceramists: Supplement no. 1. The Journal of the American Ceramic Society, 154–164.

Megaw, H.C. (1973) Crystal Structures: A Working Approach, 563 p. W.B. Saunders.

Meldrum, A., Boatner, L.A., and Ewing, R.C. (1997a) Displacive radiation effects in the monazite- and zircon-structure orthophosphates. Physical Review B: Condensed Matter and Materials Physics, 56, 13805–13814, https://doi.org/10.1103/PhysRevB.56.13805.

Meldrum, A., Boatner, L.A., Wang, L.M., and Ewing, R.C. (1997b) Ion-beam-induced amorphization of $LaPO_4$ and $ScPO_4$. Nuclear Instruments & Methods in Physics Research, Section B, Beam Interactions with Materials and Atoms, 127–128, 160–165.

Meldrum, A., Zinkle, S.J., Boatner, L.A., and Ewing, R.C. (1999) Heavy-ion irradiation effects in the ABO_4 orthosilicates: Decomposition, amorphization, and recrystallization. Physical Review B: Condensed Matter and Materials Physics, 59, 3981–3992, https://doi.org/10.1103/PhysRevB.59.3981.

Meldrum, A., Boatner, L.A., and Ewing, R.C. (2000) A comparison of radiation effects in crystalline ABO_4 -type phosphates and silicates. Mineralogical Magazine, 64, 185–194, https://doi.org/10.1180/002646100549283.

Mesbah, A., Szenknect, S., Clavier, N., Lozano-Rodriguez, J., Poinssot, C., Den Auwer, C., Ewing, R.C., and Dacheux, N. (2015) Coffinite, $USiO_4$, is abundant in nature: So why is it so difficult to synthesize? Inorganic Chemistry, 54, 6687–6696, https://doi.org/10.1021/ic502808n.

Mesbah, A., Clavier, N., Lozano-Rodriguez, M.J., Szenknect, S., and Dacheux, N. (2016) Incorporation of thorium in the zircon structure type through the $Th_{1-x}Er_x(SiO_4)_{1-x}(PO_4)_x$ thorite-xenotime solid solution. Inorganic Chemistry, 55, 11273–11282, https://doi.org/10.1021/acs.inorgchem.6b01862.

Migdisov, A., Williams-Jones, A.E., Brugger, J., and Caporuscio, F.A. (2016) Hydrothermal transport, deposition, and fractionation of the REE: Experimental data and thermodynamic calculations. Chemical Geology, 439, 13–42, https://doi.org/10.1016/j.chemgeo.2016.06.005.

Migdisov, A., Guo, X., Nisbet, H., Xu, H., and Williams-Jones, A.E. (2019) Fractionation of REE, U, and Th in natural ore-forming hydrothermal systems: Thermodynamic

modeling. The Journal of Chemical Thermodynamics, 128, 305–319, https://doi.org/10.1016/j.jct.2018.08.032.
Mihailova, B., Waeselmann, N., Stangarone, C., Angel, R.J., Prencipe, M., and Alvaro, M. (2019) The pressure-induced phase transition(s) of $ZrSiO_4$: Revised: Experimental proof for the existence of a new high-pressure polymorph of zircon. Physics and Chemistry of Minerals, 46, 807–814, https://doi.org/10.1007/s00269-019-01041-1.
Miles, N.M., Horath, D.D., and Russell, D.S. (1971) Wakefieldite, yttrium vanadate, a new mineral from Quebec. American Mineralogist, 56, 395–410.
Milligan, W.O., Mullica, D.F., Beall, G.W., and Boatner, L.A. (1982) Structural investigations of YPO_4, $ScPO_4$, and $LuPO_4$. Inorganica Chimica Acta, 60, 39–43, https://doi.org/10.1016/S0020-1693(00)91148-4.
——— (1983) The structures of three lanthanide orthophosphates. Inorganica Chimica Acta, 70, 133–136, https://doi.org/10.1016/S0020-1693(00)82791-7.
Mittal, R., Garg, A.B., Vijayakumar, V., Achary, S.N., Tyagi, A.K., Godwal, B.K., Busetto, E., Lausi, A., and Chaplot, S.L. (2008) Investigation of the phase stability of $LuVO_4$ at high pressure using powder X-ray diffraction measurements and lattice dynamical calculations. Journal of Physics: Condensed Matter, 20, 075223.
Mogilevsky, P. (2007) On the miscibility gap in monazite–xenotime systems. Physics and Chemistry of Minerals, 34, 201–214, https://doi.org/10.1007/s00269-006-0139-1.
Mogilevsky, P., Zaretsky, E.B., Parthasarathy, T.A., and Meisenkothen, F. (2006) Composition, lattice parameters, and room temperature elastic constants of natural single crystal xenotime from Novo Horizonte. Physics and Chemistry of Minerals, 33, 691–698, https://doi.org/10.1007/s00269-006-0118-6.
Momma, K. and Izumi, F. (2011) *VESTA 3* for three-dimensional visualization of crystal, volumetric and morphology data. Journal of Applied Crystallography, 44, 1272–1276, https://doi.org/10.1107/S0021889811038970.
Mondal, S.K., Das, P.K., Mandal, N., and Arya, A. (2020) A novel approach to the structural distortions of U/Th snub-disphenoids and their control on zircon → reidite type phase transitions of $U_{1-x}Th_xSiO_4$. Journal of Physics: Condensed Matter, 32, 145401, https://doi.org/10.1088/1361-648X/ab60e4.
Moriyama, T., Miyawaki, R., Yokoyama, K., Matsubara, S., Hirano, H., Murakami, H., and Watanabe, Y. (2011) Wakefieldite-Nd a new neodymium vanadate mineral in the Arase Stratiform Ferromanganese Deposit, Kochi Prefecture, Japan. Resource Geology, 61, 101–110, https://doi.org/10.1111/j.1751-3928.2010.00151.x.
Morss, L.R., Day, P.P., Felinto, C., and Brito, H. (1993) Standard molar enthalpies of formation of Y_2O_3, Ho_2O_3, and Er_2O_3 at the temperature 298.15 K. The Journal of Chemical Thermodynamics, 25, 415–422, https://doi.org/10.1006/jcht.1993.1045.
Moura, M.R., Ayala, A.P., Guedes, I., Grimsditch, M., Loong, C.K., and Boatner, L.A. (2004) Raman scattering study of $Tb(V_{1-x}P_x)O_4$ single crystals. Journal of Applied Physics, 95, 1148–1151, https://doi.org/10.1063/1.1640461.
Mrose, M.E. and Rose, J. Jr. (1961) Béhierite,(Ta, Nb)BO_4, a new mineral from Manjaka, 111. Geological Society of America.
Mulak, J. (1977) Crystal field parameters in $USiO_4$ from temperature dependence of paramagnetic susceptibility. Journal of Solid State Chemistry, 21, 117–126, https://doi.org/10.1016/0022-4596(77)90151-7.
Muller, O., White, W.B., and Roy, R. (1969) X-ray diffraction study of the chromates of nickel, magnesium, and cadmium. Zeitschrift für Kristallographie, 130, 112–120, https://doi.org/10.1524/zkri.1969.130.1-6.112.
Mullica, D.F., Sappenfield, E.L., and Boatner, L.A. (1996a) Monazite- and zircon-type structures of seven mixed (Ln/Ln)PO_4 compounds. Inorganica Chimica Acta, 244, 247–252, https://doi.org/10.1016/0020-1693(95)04783-2.
Mullica, D.F., Sappenfield, E.L., Abraham, M.M., Chakoumakos, B.C., and Boatner, L.A. (1996b) Structural investigations of several $LnVO_4$ compounds. Inorganica Chimica Acta, 248, 85–88, https://doi.org/10.1016/0020-1693(95)04971-1.
Mumpton, F.A. and Roy, R. (1961) Hydrothermal stability studies of the zircon-thorite group. Geochimica et Cosmochimica Acta, 21, 217–238, https://doi.org/10.1016/S0016-7037(61)80056-2.
Murakami, T., Chakoumakos, B.C., Ewing, R.C., Lumpkin, G.R., and Weber, W.J. (1991) Alpha-decay event damage in zircon. American Mineralogist, 76, 1510–1532.
Mursic, Z., Vogt, T., and Frey, F. (1992) High-temperature neutron powder diffraction study of $ZrSiO_4$ up to 1900 K. Acta Crystallographica Section B, 48, 584–590, https://doi.org/10.1107/S0108768192002982.
Musselman, M.A., Wilkinson, T.M., Haberl, B., and Packard, C.E. (2018) In situ Raman spectroscopy of pressure-induced phase transformations in polycrystalline $TbPO_4$, $DyPO_4$, and $Gd_xDy_{(1-x)}PO_4$. Journal of the American Ceramic Society, 101, 2562–2570, https://doi.org/10.1111/jace.15374.
Nasdala, L., Zhang, M., Kempe, U., Panczer, G., Gaft, M., Andrut, M., and Plötze, M. (2003) Spectroscopic methods applied to zircon. In J.M. Hanchar and P.W.O. Hoskin, Eds., Zircon, 53, 427–468. Reviews in Mineralogy and Geochemistry, Mineralogical Society of America, Chantilly, Virginia.
Navrotsky, A. (1994) Physics and Chemistry of Earth Materials, 432 p. Cambridge University Press.
——— (2001) Systematic trends and prediction of enthalpies of formation of refractory lanthanide and actinide ternary oxide phases. Ceramic Transactions, 137–146.
——— (2005) Thermochemical insights into refractory ceramic materials based on oxides with large tetravalent cations. Journal of Materials Chemistry, 15, 1883–1890, https://doi.org/10.1039/b417143h.
Navrotsky, A. and Ushakov, S.V. (2005) Materials Fundamentals of Gate Dielectrics, 484 p. Springer.
Navrotsky, A., Lee, W., Mielewczyk-Gryn, A., Ushakov, S.V., Anderko, A., Wu, H., and Riman, R.E. (2015) Thermodynamics of solid phases containing rare earth oxides. The Journal of Chemical Thermodynamics, 88, 126–141, https://doi.org/10.1016/j.jct.2015.04.008.
Neves, J.M.C., Nunes, J.E.L., and Sahama, T.G. (1974) High hafnium members of the zircon-hafnon series from the granite pegmatites of Zambézia, Mozambique. Contributions to Mineralogy and Petrology, 48, 73–80, https://doi.org/10.1007/BF00399111.
Newnham, R.E. (2005) Properties of Materials, 390 p. Oxford University Press.
Newton, R.C., Manning, C.E., Hanchar, J.M., and Finch, R.J. (2005) Gibbs free energy of formation of zircon from measurement of solubility in H_2O. Journal of the American Ceramic Society, 88, 1854–1858, https://doi.org/10.1111/j.1551-2916.2005.00348.x.
Ni, Y., Hughes, J.M., and Mariano, A.N. (1995) Crystal chemistry of the monazite and xenotime structures. American Mineralogist, 80, 21–26, https://doi.org/10.2138/am-1995-1-203.
Ono, S., Tange, Y., Katayama, I., and Kikegawa, T. (2004a) Equation of state of $ZrSiO_4$ phases in the upper mantle. American Mineralogist, 89, 185–188, https://doi.org/10.2138/am-2004-0121.
Ono, S., Funakoshi, K., Nakajima, Y., Tange, Y., and Katsura, T. (2004b) Phase transition of zircon at high *P-T* conditions. Contributions to Mineralogy and Petrology, 147, 505–509, https://doi.org/10.1007/s00410-004-0570-6.
Orlova, A.I. and Ojovan, M.I. (2019) Ceramic mineral waste-forms for nuclear waste immobilization. Materials (Basel), 12, 2638, https://doi.org/10.3390/ma12162638.
Panchal, V., Errandonea, D., Segura, A., Rodríguez-Hernandez, P., Muñoz, A., Lopez-Moreno, S., and Bettinelli, M. (2011a) The electronic structure of zircon-type orthovanadates: Effects of high-pressure and cation substitution. Journal of Applied Physics, 110, 043723, https://doi.org/10.1063/1.3626060.
Panchal, V., López-Moreno, S., Santamaría-Pérez, D., Errandonea, D., Manjón, F.J., Rodríguez-Hernandez, P., Muñoz, A., Achary, S.N., and Tyagi, A.K. (2011b) Zircon to monazite phase transition in $CeVO_4$: X-ray diffraction and Raman-scattering measurements. Physical Review B: Condensed Matter and Materials Physics, 84, 024111, https://doi.org/10.1103/PhysRevB.84.024111.
Panchal, V., Errandonea, D., Manjón, F.J., Muñoz, A., Rodríguez-Hernández, P., Bettinelli, M., Achary, S.N., and Tyagi, A.K. (2015) High pressure phase transitions in $NdVO_4$. AIP Conference Proceedings, 1665, 030006.
Parker, R.L. and Fleischer, M. (1968) Geochemistry of Niobium and Tantalum. Geological Survey Professional Paper 612. U.S. Department of the Interior.
Paszkowicz, W., Ermakova, O., López-Solano, J., Mujica, A., Muñoz, A., Minikayev, R., Lathe, C., Gierlotka, S., Nikolaenko, I., and Dabkowska, H. (2014) Equation of state of zircon- and scheelite-type dysprosium orthovanadates: A combined experimental and theoretical study. Journal of Physics: Condensed Matter, 26, 025401, https://doi.org/10.1088/0953-8984/26/2/025401.
Pointeau, V., Deditius, A.P., Miserque, F., Renock, D., Becker, U., Zhang, J., Clavier, N., Dacheux, N., Poinssot, C., and Ewing, R.C. (2009) Synthesis and characterization of coffinite. Journal of Nuclear Materials, 393, 449–458, https://doi.org/10.1016/j.jnucmat.2009.06.030.
Popescu, C., Garg, A.B., Errandonea, D., Sans, J.A., Rodriguez-Hernández, P., Radescu, S., Muñoz, A., Achary, S.N., and Tyagi, A.K. (2016) Pressure-induced phase transformation in zircon-type orthovanadate $SmVO_4$ from experiment and theory. Journal of Physics: Condensed Matter, 28, 035402, https://doi.org/10.1088/0953-8984/28/3/035402.
Prieur, D., Bonani, W., Popa, K., Walter, O., Kriegsman, K.W., Engelhard, M.H., Guo, X., Eloirdi, R., Gouder, T., Beck, A., and others. (2020) Size dependence of lattice parameter and electronic structure in CeO_2 nanoparticles. Inorganic Chemistry, 59, 5760–5767, https://doi.org/10.1021/acs.inorgchem.0c00506.
Qi, J., Guo, X., Mielewczyk-Gryn, A., and Navrotsky, A. (2015) Formation enthalpies of $LaLnO_3$ (Ln=Ho, Er, Tm and Yb) interlanthanide perovskites. Journal of Solid State Chemistry, 227, 150–154, https://doi.org/10.1016/j.jssc.2015.03.026.
Rafiuddin, M.R. and Grosvenor, A.P. (2015) Probing the effect of radiation damage on the structure of rare-earth phosphates. Journal of Alloys and Compounds, 653, 279–289, https://doi.org/10.1016/j.jallcom.2015.08.276.
Rafiuddin, M.R., Seydoux-Guillaume, A.M., Deschanels, X., Mesbah, A., Baumier, C., Szenknect, S., and Dacheux, N. (2020) An in-situ electron microscopy study of dual ion-beam irradiated xenotime-type $ErPO_4$. Journal of Nuclear Materials, 539, 152265, https://doi.org/10.1016/j.jnucmat.2020.152265.
Range, K.-J., Wildenauer, M., and Heyns, A.M. (1988) Extrem kurze nichtbindende Sauerstoff-Sauerstoff-Abstände: Die Kristallstrukturen von $NbBO_4$, $NaNb_2O_6$ und $NaTa_3O_8$. Angewandte Chemie, 100, 973–975, https://doi.org/10.1002/ange.19881000721.
Range, K.J., Wildenauer, M., and Andratshke, M. (1996) Crystal structure of tantalum orthoborate, $TaBO_4$. Zeitschrift für Kristallographie, 211, 815.
Reid, A.F. and Ringwood, A.E. (1969) Newly observed high pressure transformation in Mn_3O_4, $CaAl_2O_4$, and $ZrSiO_4$. Earth and Planetary Science Letters, 6, 205–208, https://doi.org/10.1016/0012-821X(69)90091-0.
Reynolds, H.S. (2013) Synthesis, characterisation and dissolution studies of the uranium mineral coffinite. Ph.D. thesis, Royal Melbourne Institute of Technology University.
Ridley, M., McFarland, B., Miller, C., and Opila, E. (2022) $YbPO_4$: A novel environmental barrier coating candidate with superior thermochemical stability. Materialia, 21, 101289, https://doi.org/10.1016/j.mtla.2021.101289.
Robie, R.A. and Hemingway, B.S. (1995) Thermodynamic Properties of minerals and related substances at 298.15 K and 1 bar (10^5 pascals) pressure and at higher tem-

peratures. U.S. Geological Survey Bulletin, 2131, https://doi.org/10.3133/b2131.
Robinson, K., Gibbs, G.V., and Ribbe, P.H. (1971) The structure of zircon: A comparison with garnet. American Mineralogist, 56, 782–790.
Rubatto, D. and Hermann, J. (2007) Experimental zircon/melt and zircon/garnet trace element partitioning and implications for the geochronology of crustal rocks. Chemical Geology, 241, 38–61, https://doi.org/10.1016/j.chemgeo.2007.01.027.
Ruiz-Fuertes, J., Martínez-García, D., Marqueño, T., Errandonea, D., MacLeod, S.G., Bernert, T., Haussühl, E., Santamaría-Pérez, D., Ibáñez, J., Mallavarapu, A., and others. (2018) High-pressure high-temperature stability and thermal equation of state of zircon-type erbium vanadate. Inorganic Chemistry, 57, 14005–14012, https://doi.org/10.1021/acs.inorgchem.8b01808.
Ryumin, M.A., Gurevich, V.M., Khoroshilov, A.V., Tyurin, A.V., and Gavrichev, K.S. (2017) Heat capacity and thermodynamic functions of thulium orthophosphate $TmPO_4$ in the range of 10–1350 K. Russian Journal of Physical Chemistry A, Focus on Chemistry, 91, 2310–2316, https://doi.org/10.1134/S003602441711019X.
Sáez-Puche, R., Jiménez, E., Isasi, J., Fernández-Díaz, M.T., and García-Muñoz, J.L. (2003) Structural and magnetic characterization of $RCrO_4$ oxides (R = Nd, Er and Tm). Journal of Solid State Chemistry, 171, 161–169, https://doi.org/10.1016/S0022-4596(02)00203-7.
Sáez Puche, R., Gallardo, J.M., de Paz, R.J., Taira, N., and Climent-Pascual, E. (2009) Structural phase transitions zircon to scheelite type induced by pressure in the $RCrO_4$ oxides (R=rare earth). The Journal of Argentine Chemical Society, 97, 90–101.
Santos, C.C., Silva, E.N., Ayala, A.P., Guedes, I., Pizani, P.S., Loong, C.K., and Boatner, L.A. (2007) Raman investigations of rare earth orthovanadates. Journal of Applied Physics, 101, 053511, https://doi.org/10.1063/1.2437676.
Schafer, W. and Will, G. (1971) Neutron diffraction study of antiferromagnetic $DyAsO_4$. Journal of Physics C, Solid State Physics, 4, 3224–3233, https://doi.org/10.1088/0022-3719/4/18/028.
Schäfer, W., Will, G., and Müller-Vogt, G. (1979) Refinement of the crystal structure of terbium arsenate $TbAsO_4$ at 77 K and 5 K by profile analysis from neutron diffraction powder data. Acta Crystallographica Section B, 35, 588–592, https://doi.org/10.1107/S0567740879004210.
Schlüter, J., Malcherek, T., and Husdal, T.A. (2009) The new mineral stetindite, $CeSiO_4$, a cerium end-member of the zircon group. Neues Jahrbuch für Mineralogie. Abhandlungen, 186, 195–200, https://doi.org/10.1127/0077-7757/2009/0146.
Schmidt, M., Müller, U., Cardoso Gil, R., Milke, E., and Binnewies, M. (2005) Zum chemischen transport und zur kristallstruktur von seltenerdarsenaten(V). Zeitschrift für Anorganische und Allgemeine Chemie, 631, 1154–1162, https://doi.org/10.1002/zaac.200400544.
Schuiling, R.D., Vergouwen, L., and van der Rijst, H. (1976) Gibbs energies of formation of zircon ($ZrSiO_4$), thorite ($ThSiO_4$), and phenacite (Be_2SiO_4). American Mineralogist, 61, 166–168.
Schulz, K. and Papp, J.F. (2014) Niobium and Tantalum—Indispensable Twins. USGS Mineral Resources Program, 5–6.
Seydoux, A.M. and Montel, J.M. (1997) Experimental determination of the thorite-huttonite phase transition. EUG IX, Terra Nova 9, Abstract Supplement, 1.
Shannon, R.D. (1976) Revised effective ionic radii and systematic studies of interatomic distances in halides and chalcogenides. Acta Crystallographica Section A, 32, 751–767, https://doi.org/10.1107/S0567739476001551.
Shein, I.R., Shein, K.I., and Ivanovskii, A.L. (2006) Thorite versus huttonite: Stability, electronic properties and X-ray emission spectra from first-principle calculations. Physics and Chemistry of Minerals, 33, 545–552, https://doi.org/10.1007/s00269-006-0100-3.
Shelyug, A., Rafiuddin, M.R., Mesbah, A., Clavier, N., Szenknect, S., Dacheux, N., Guo, X., and Navrotsky, A. (2021) Effect of annealing on structural and thermodynamic properties of $ThSiO_4$-$ErPO_4$ xenotime solid solution. Inorganic Chemistry, 60, 12020–12028, https://doi.org/10.1021/acs.inorgchem.1c01137.
Shin, D., Arróyave, R., and Liu, Z.K. (2006) Thermodynamic modeling of the Hf-Si-O system. Calphad, 30, 375–386, https://doi.org/10.1016/j.calphad.2006.08.006.
Skakle, J.M.S., Dickson, C.L., and Glasser, F.P. (2000) The crystal structures of $CeSiO_4$ and $Ca_2Ce_8(SiO_4)_6O_2$. Powder Diffraction, 15, 234–238, https://doi.org/10.1017/S0885715600011143.
Speer, J.A. (1980a) The actinide orthosilicates. Reviews in Mineralogy and Geochemistry, 5, 113–135.
——— (1980b) Zircon. Reviews in Mineralogy and Geochemistry, 5, 67–112.
Speer, J.A. and Cooper, B.J. (1982) Crystal structure of synthetic hafnon, $HfSiO_4$, comparison with zircon and the actinide orthosilicates. American Mineralogist, 67, 804–808.
Stangarone, C., Angel, R.J., Prencipe, M., Mihailova, B., and Alvaro, M. (2019) New insights into the zircon-reidite phase transition. American Mineralogist, 104, 830–837, https://doi.org/10.2138/am-2019-6827.
Stavrou, E., Tatsi, A., Salpea, E., Boulmetis, Y.C., Kontos, A.G., Raptis, Y.S., and Raptis, C. (2008) Raman study of zircon-structured RPO_4 (R = Y, Tb, Er, Tm) phosphates at high pressures. Journal of Physics: Conference Series, 121, 042016, https://doi.org/10.1088/1742-6596/121/4/042016.
Stieff, L.R., Stern, T.W., and Sherwood, A.M. (1955) Preliminary description of coffinite—A new uranium mineral. Science, 121, 608–609, https://doi.org/10.1126/science.121.3147.608.b.
——— (1956) Coffinite, A uranous silicate with hydroxyl subsitution: A new mineral. American Mineralogist, 41, 675–688.
Strzelecki, A.C., Kriegsman, K.W., Estevenon, P., Goncharov, V., Bai, J., Szenknect, S., Mesbah, A., Wu, D., McCloy, J.S., Dacheux, N., and others. (2020a) High-temperature thermodynamics of cerium silicates, A-$Ce_2Si_2O_7$ and $Ce_{4.67}(SiO_4)_3O$. ACS Earth & Space Chemistry, 4, 2129–2143, https://doi.org/10.1021/acsearthspacechem.0c00231.
Strzelecki, A.C., Bourgeois, C., Kriegsman, K.W., Estevenon, P., Wei, N., Szenknect, S., Mesbah, A., Wu, D., Ewing, R.C., Dacheux, N., and others. (2020b) Thermodynamics of $CeSiO_4$: Implications for actinide orthosilicates. Inorganic Chemistry, 59, 13174–13183, https://doi.org/10.1021/acs.inorgchem.0c01476.
Strzelecki, A.C., Barral, T., Estevenon, P., Mesbah, A., Goncharov, V., Baker, J., Bai, J., Clavier, N., Szenknect, S., Migdisov, A., and others. (2021) The role of water and hydroxyl groups in the structures of stetindite and coffinite, $MSiO_4$ (M = Ce, U). Inorganic Chemistry, 60, 718–735, https://doi.org/10.1021/acs.inorgchem.0c02757.
Strzelecki, A.C., Reece, M.E., Zhao, X., Yu, W., Benmore, C.J., Ren, Y., Alcorn, C.D., Migdisov, A., Xu, H., and Guo, X. (2022) Thermodynamics of mixing HREE in xenotime solid solution ($Er_{(x)}Yb_{(1-x)}PO_4$). ACS Earth & Space Chemistry, 4, 2461–2469.
Strzelecki, A.C., Zhao, X., Baker, J.L., Estevenon, P., Barral, T., Mesbah, A., Popov, D., Chariton, S., Prakapenka, V., Ahmed, S., and others. (2023) High-pressure structural and thermodynamic properties of cerium orthosilicates ($CeSiO_4$). The Journal of Physical Chemistry. C, Nanomaterials and Interfaces, 127, 4225–4238, https://doi.org/10.1021/acs.jpcc.2c06657.
Su, L., Wan, L., Gao, T., and Ao, B. (2020) First-principles calculations of the electronic structure, chemical bonding, and thermodynamic properties of $USiO_4$. AIP Advances, 10, 075018, https://doi.org/10.1063/5.0018203.
Subbarao, E.C., Agrawal, D.K., McKinstry, H.A., Sallese, C.W., and Roy, R. (1990) Thermal expansion of compounds of zircon structure. Journal of the American Ceramic Society, 73, 1246–1252, https://doi.org/10.1111/j.1151-2916.1990.tb05187.x.
Sverjensky, D.A. and Molling, P.A. (1992) A linear free energy relationship for crystalline solids and aqueous ions. Nature, 356, 231–234, https://doi.org/10.1038/356231a0.
Sverjensky, D.A., Shock, E.L., and Helgeson, H.C. (1997) Prediction of the thermodynamic properties of aqueous metal complexes to 1000 °C and 5 kb. Geochimica et Cosmochimica Acta, 61, 1359–1412, https://doi.org/10.1016/S0016-7037(97)00009-4.
Syverson, D.D., Etschmann, B., Liu, W., Ram, R., Mei, Y., Lanzirotti, T., Mercadier, J., and Brugger, J. (2019) Oxidation state and coordination environment of Pb in U-bearing minerals. Geochimica et Cosmochimica Acta, 265, 109–131, https://doi.org/10.1016/j.gca.2019.08.039.
Szenknect, S., Costin, D.T., Clavier, N., Mesbah, A., Poinssot, C., Vitorge, P., and Dacheux, N. (2013) From uranothorites to coffinite: A solid solution route to the thermodynamic properties of $USiO_4$. Inorganic Chemistry, 52, 6957–6968, https://doi.org/10.1021/ic400272s.
Szenknect, S., Mesbah, A., Cordara, T., Clavier, N., Brau, H.P., Le Goff, X., Poinssot, C., Ewing, R.C., and Dacheux, N. (2016) First experimental determination of the solubility constant of coffinite. Geochimica et Cosmochimica Acta, 181, 36–53, https://doi.org/10.1016/j.gca.2016.02.010.
Tanaka, K., Takahashi, Y., Horie, K., Shimizu, H., and Murakami, T. (2010) Determination of the oxidation state of radiogenic Pb in natural zircon using X-ray absorption near-edge structure. Physics and Chemistry of Minerals, 37, 249–254, https://doi.org/10.1007/s00269-009-0330-2.
Tananaev, I.V., Orlovsky, V.P., Kurbanov, J.M., Halikov, B.S., Osman, S.O., and Bulgakov, V.I. (1974) Reports of the Academy of Sciences of the Tajik SSR, 42 p.
Tange, Y. and Takahashi, E. (2004) Stability of the high-pressure polymorph of zircon ($ZrSiO_4$) in the deep mantle. Physics of the Earth and Planetary Interiors, 143-144, 223–229, https://doi.org/10.1016/j.pepi.2003.10.009.
Taylor, M. and Ewing, R.C. (1978) The crystal structures of the $ThSiO_4$ polymorphs: Huttonite and thorite. Acta Crystallographica. Section B, 34, 1074–1079, https://doi.org/10.1107/S0567740878004951.
Tezuka, K. and Hinatsu, Y. (2001) Magnetic and crystallographic properties of $LnCrO_4$ (Ln=Nd, Sm, and Dy). Journal of Solid State Chemistry, 160, 362–367, https://doi.org/10.1006/jssc.2001.9241.
Tezuka, K., Doi, Y., and Hinatsu, Y. (2002) Crystal structures and magnetic properties of zircon-type compounds $Lu_{1-x}Y_xCrO_4$. Journal of Materials Chemistry, 12, 1189–1193, https://doi.org/10.1039/b108483f.
Tyurin, A.V., Ryumin, M.A., Khoroshilov, A.V., Gurevich, V.M., and Gavrichev, K.S. (2020) Thermodynamic functions of holmium orthophosphate $HoPO_4$ in the range 9–1370 K. Thermochimica Acta, 683, 178459, https://doi.org/10.1016/j.tca.2019.178459.
Ushakov, S.V., Helean, K.B., Navrotsky, A., and Boatner, L.A. (2001a) Thermochemistry of rare-earth orthophosphates. Journal of Materials Research, 16, 2623–2633, https://doi.org/10.1557/JMR.2001.0361.
Ushakov, S.V., Helean, K.B., Navrotsky, A., and Boatner, L.A. (2001b) Thermochemistry of rare-earth orthophosphates. Journal of Materials Research, 16, 2623–2633.
Valley, J.W. (2003) Oxygen isotopes in zircon. In J.M. Hanchar and P.W.O. Hoskin, Eds., Zircon, 53, 343–386. Reviews in Mineralogy and Geochemistry, Mineralogical Society of America, Chantilly, Virginia.
Van Hoozen, C.J., Gysi, A.P., and Harlov, D.E. (2020) The solubility of monazite ($LaPO_4$, $PrPO_4$, $NdPO_4$, and $EuPO_4$) endmembers in aqueous solutions from 100 to 250 °C. Geochimica et Cosmochimica Acta, 280, 302–316, https://doi.org/10.1016/j.gca.2020.04.019.

Van Westrenen, W., Frank, M.R., Hanchar, J.M., Fei, Y., Finch, R.J., and Zha, C.-S. (2004) In situ determination of the compressibility of synthetic pure zircon ($ZrSiO_4$) and the onset of the zircon-reidite phase transformation. American Mineralogist, 89, 197–203, https://doi.org/10.2138/am-2004-0123.

Varghese, J., Joseph, T., Surendran, K.P., Rajan, T.P.D., and Sebastian, M.T. (2015) Hafnium silicate: A new microwave dielectric ceramic with low thermal expansivity. Dalton Transactions, 44, 5146–5152, https://doi.org/10.1039/C4DT03367A.

Vitova, T., Pidchenko, I., Fellhauer, D., Bagus, P.S., Joly, Y., Pruessmann, T., Bahl, S., Gonzalez-Robles, E., Rothe, J., Altmaier, M., and others. (2017) The role of the 5f valence orbitals of early actinides in chemical bonding. Nature Communications, 8, 16053, https://doi.org/10.1038/ncomms16053.

Wang, X., Loa, I., Syassen, K., Hanfland, M., and Ferrand, B. (2004) Structural properties of the zircon- and scheelite-type phases of YVO_4 at high pressure. Physical Review B: Condensed Matter and Materials Physics, 70, 3–8.

Wang, Y., Chen, X., Liu, W., Cheng, L., and Zhang, L. (2010) Exploration of YPO_4 as a potential environmental barrier coating. Ceramics International, 36, 755–759, https://doi.org/10.1016/j.ceramint.2009.10.014.

Watson, E.B., Chemiak, D.J., Hanchar, J.M., Harrison, T.M., and Wark, D.A. (1997) The incorporation of Pb into zircon. Chemical Geology, 141, 19–31, https://doi.org/10.1016/S0009-2541(97)00054-5.

Watson, E.B., Wark, D.A., and Thomas, J.B. (2006) Crystallization thermometers for zircon and rutile. Contributions to Mineralogy and Petrology, 151, 413–433, https://doi.org/10.1007/s00410-006-0068-5.

Weber, W.J. (1991) Self-radiation damage and recovery in Pu-doped zircon. Radiation Effects and Defects in Solids, 115, 341–349, https://doi.org/10.1080/10420159108220580.

——— (1993) Alpha-decay-induced amorphization in complex silicate structures. Journal of the American Ceramic Society, 76, 1729–1738, https://doi.org/10.1111/j.1151-2916.1993.tb06641.x.

Weber, W.J. and Ewing, R.C. (2013) Ceramic waste forms for uranium and transuranium elements. In P.C. Burns and G.E. Sigmon, Eds., Uranium: Cradle to Grave, 317–336. Mineralogical Association of Canada.

Weber, G. and Range, K.J. (1996) Notizen: Die kristallstruktur von calciumchromat(VI), $CaCrO_4$/The crystal structure of calcium chromate (VI), $CaCrO_4$. Zeitschrift für Naturforschung. Section B. A Journal of Chemical Sciences, 51, 751–753, https://doi.org/10.1515/znb-1996-0523.

Weber, W.J., Ewing, R.C., and Wang, L.M. (1994) The radiation-induced crystalline-to-amorphous transition in zircon. Journal of Materials Research, 9, 688–698, https://doi.org/10.1557/JMR.1994.0688.

Weber, W.J., Ewing, R.C., and Lutze, W. (1995) Performance assessment of zircon as a waste form for excess weapons plutonium under deep borehole burial conditions. Proceedings of the Materials Research Society, 412, 25–32, https://doi.org/10.1557/PROC-412-25.

Weber, W.J., Ewing, R.C., Catlow, C.R.A., Diaz De La Rubia, T., Hobbs, L.W., Kinoshita, C., Matzke, H., Motta, A.T., Nastasi, M., Salje, E.K.H., and others. (1998) Radiation effects in crystalline ceramics for the immobilization of high-level nuclear waste and plutonium. Journal of Materials Research, 13, 1434–1484, https://doi.org/10.1557/JMR.1998.0205.

Weber, W.J., Navrotsky, A., Stefanovsky, S., Vance, E.R., and Vernaz, E. (2009) Materials science of high-level nuclear waste immobilization. MRS Bulletin, 34, 46–53, https://doi.org/10.1557/mrs2009.12.

Weber, W.J., Ewing, R.C., Vance, E.R., Gregg, D., Peuget, S., and Wiss, T. (2019) Plutonium in waste forms. In D.L. Clark, D.A. Geeson, and R.J. Hanrahan Jr., Eds., Plutonium Handbook, 2349–2422. American Nuclear Society.

Wegel, S., Czempinski, V., Oei, P.-Y., and Wealer, B. (2019) Transporting and storing high-level nuclear waste in the U.S.-insights from a mathematical model. Applied Sciences (Basel, Switzerland), 9, 2437, https://doi.org/10.3390/app9122437.

West, A. (2014) Solid State Chemistry and Its Application, 2nd edition, 592 p. Wiley.

White, W.M. (2015) Isotope Geochemistry, 496 p. Wiley-Blackwell.

Witzke, T., Kolitsch, U., and Warnsloh, J.M.G. (2008) Wakefieldite-(La), $LaVO_4$, a new mineral species from the Glucksstern Mine, Friedrichroda, Thuringia, Germany. European Journal of Mineralogy, 20, 1135–1139, https://doi.org/10.1127/0935-1221/2009/0021-1875.

Xu, H., Zhao, Y., Zhang, J., Wang, Y., Hickmott, D.D., Daemen, L.L., Hartl, M.A., and Wang, L. (2010a) Anisotropic elasticity of jarosite: A high-P synchrotron XRD study. American Mineralogist, 95, 19–23, https://doi.org/10.2138/am.2010.3280.

Xu, H., Zhao, Y., Vogel, S.C., Hickmott, D.D., Daemen, L.L., and Hartl, M.A. (2010b) Thermal expansion and decomposition of jarosite: A high-temperature neutron diffraction study. Physics and Chemistry of Minerals, 37, 73–82, https://doi.org/10.1007/s00269-009-0311-5.

Yue, B., Hong, F., Merkel, S., Tan, D., Yan, J., Chen, B., and Mao, H.K. (2016) Deformation behavior across the zircon-scheelite phase transition. Physical Review Letters, 117, 135701, https://doi.org/10.1103/PhysRevLett.117.135701.

Zhang, F.X., Lang, M., Ewing, R.C., Lian, J., Wang, Z.W., Hu, J., and Boatner, L.A. (2008a) Pressure-induced zircon-type to scheelite-type phase transitions in $YbPO_4$ and $LuPO_4$. Journal of Solid State Chemistry, 181, 2633–2638, https://doi.org/10.1016/j.jssc.2008.06.042.

Zhang, M., Boatner, L.A., Salje, E.K.H., Honda, S., and Ewing, R.C. (2008b) Pb^+ irradiation of synthetic zircon ($ZrSiO_4$): Infrared spectroscopic investigation. American Mineralogist, 93, 1418–1423, https://doi.org/10.2138/am.2008.2733.

Zhang, F.X., Pointeau, V., Shuller, L.C., Reaman, D.M., Lang, M., Liu, Z., Hu, J., Panero, W.R., Becker, U., Poinssot, C., and others. (2009) Structural transitions and electron transfer in coffinite, $USiO_4$, at high pressure. American Mineralogist, 94, 916–920, https://doi.org/10.2138/am.2009.3111.

Manuscript received June 7, 2022
Manuscript accepted April 5, 2023
Accepted manuscript online April 21, 2023
Manuscript handled by Daniel E. Harlov

Endnote:

[1]Deposit item AM-24-28632. Online Materials are free to all readers. Go online, via the table of contents or article view, and find the tab or link for supplemental materials.